

1 Dear Dr. Combourieu-Nebout,
2
3 We submit for your consideration the fourth version of our manuscript "A Stalagmite Test of North
4 Atlantic SST and Iberian Hydroclimate Linkages over the Last Two Glacial Cycles", which now
5 contains all of the changes recommended by you based on the last iteration of this work. Your
6 suggestions were insightful and detailed, and we appreciate them.
7
8 Sincerely,
9 Rhawn Denniston

A Stalagmite Test of North Atlantic SST and Iberian Hydroclimate Linkages over the Last Two Glacial Cycles

Rhawn F. Denniston^{a*}, Amanda N. Houts^{a1}, Yemane Asmerom^b, Alan D. Wanamaker, Jr.^c, Jonathon A. Haws^d, Victor J. Polyak^b, Diana L. Thatcher^c, Setsen Altan-Ochir^a, Alyssa C. Borowske^{a2}, Sebastian F.M. Breitenbach^e, Caroline C. Ummenhofer^f, Frederico T. Regala^g, Michael M. Benedetti^h, Nuno Bichoⁱ

^a Department of Geology, Cornell College, Mount Vernon, Iowa 52314 USA

^b Department of Earth and Planetary Sciences, University of New Mexico, Albuquerque, New Mexico 87131 USA

^c Department of Geological and Atmospheric Sciences, Iowa State University, Ames, Iowa 50011 USA

^d Department of Anthropology, Louisville University, Louisville, Kentucky 40208 USA

^e Institute for Geology, Mineralogy, and Geophysics, Ruhr-University Bochum 44801 Germany

^f Department of Physical Oceanography, Woods Hole Oceanographic Institution, Woods Hole, Massachusetts 02543 USA

^g Associação de Estudos Subterrâneos e Defesa do Ambiente, Torres Vedras, Portugal

^h Department of Geography and Geology, University of North Carolina Wilmington, Wilmington, North Carolina 28403 USA

ⁱ Center for Archaeology and Evolution of Human Behaviour, Universidade do Algarve, Faro, Portugal

* corresponding author

¹ current address: Department of Earth Sciences, University of New Hampshire, Durham, New Hampshire 03824 USA

² current address: Department of Ecology and Evolutionary Biology, University of Connecticut, Storrs, Connecticut 06269 USA

Keywords

Iberia, hydroclimate, stalagmite, oxygen isotope, carbon isotope, $\delta^{234}\text{U}$, pollen, sea surface temperature

45 Abstract

46 Close coupling of Iberian hydroclimate and North Atlantic sea surface temperature (SST)
47 during recent glacial periods has been identified through the analysis of marine sediment and
48 pollen grains co-deposited on the Portuguese continental margin. While offering precisely
49 correlatable records, these time series have lacked a directly-dated, site-specific record of
50 continental Iberian climate spanning multiple glacial cycles as a point of comparison. Here we
51 present a high-resolution, multi-proxy (growth dynamics and $\delta^{13}\text{C}$, $\delta^{18}\text{O}$, and $\delta^{234}\text{U}$ values)
52 composite stalagmite record of hydroclimate from two caves in western Portugal across the
53 majority of the last two glacial cycles (~220 ka). At orbital and millennial scales, stalagmite-
54 based proxies for hydroclimate covaried with SST, with elevated $\delta^{13}\text{C}$, $\delta^{18}\text{O}$, and $\delta^{234}\text{U}$
55 values and/or growth hiatuses indicating reduced effective moisture coincident with periods of
56 lowered SST during major ice-rafted debris events, in agreement with changes in palynological
57 reconstructions of continental climate. While in many cases the Portuguese stalagmite record can
58 be scaled to SST, in some intervals the magnitudes of stalagmite isotopic shifts, and possibly
59 hydroclimate, appear to have been decoupled from SST.

60

61 1. Introduction

62 The Portuguese continental margin is an important location for understanding variations
63 in paleoceanographic conditions over orbital and millennial-scales (Hodell et al., 2013; Voelker
64 and de Abreu, 2011). Here, marine sediments record basin-wide oceanographic signals while co-
65 deposited pollen grains track coeval vegetation changes occurring across Iberia. Integrated
66 analysis of these proxies has revealed a close coupling of North Atlantic SST, regional climate,
67 and Iberian ecosystems during the last three glacial cycles, including changes in vegetation
68 dynamics (Sánchez Goñi et al., 2002; Tzedakis et al., 2004; Roucoux et al., 2006; Martrat et al.,
69 2007; Naughton et al., 2007; Sánchez Goñi et al., 2008), atmospheric circulation (Sánchez Goñi
70 et al., 2013), and fire frequency (Daniau et al., 2007). One commonly applied palynological
71 metric is the abundance of temperate tree pollen, which rises during warm and wet conditions
72 associated both with interglacials and Greenland interstadials, concomitant with shifts in Iberian
73 margin SST (Sánchez Goñi et al., 2002; Tzedakis et al., 2004; Combourieu-Nebout et al., 2009;
74 Fletcher et al., 2010; Chabaud et al., 2014). However, the nature of such land-sea connections is
75 partially obscured by the size of catchments from which the pollen are derived, with some

Rhawn Denniston 11/13/2018 4:16 PM
Deleted: 230

77 reaching into central Iberia and spanning a range of environmental settings subject to varying
78 climatic influences (Martin-Vide and Lopez-Bustins, 2006; Naughton et al., 2007) (Fig. 1).

79 Testing the links between terrestrial and marine systems benefits from continental climate
80 archives that provide precisely-dated and high resolution rainfall-sensitive time series spanning
81 tens of millennia, but such records remain rare in Iberia, particularly near the west Iberian
82 margin (Fletcher et al., 2010; Moreno et al., 2012; Stoll et al., 2013). Here we present a
83 composite stalagmite record of four proxies for hydroclimate – growth dynamics and $\delta^{13}\text{C}$, $\delta^{18}\text{O}$,
84 and $\delta^{234}\text{U}$ values – spanning the majority of the last and penultimate glacial cycles (~ 220 ka) at
85 two cave sites in western Portugal. These time series offer a rare, site-specific continental record
86 capable of examining the coherence of SST controls on Iberian climate and ecosystem dynamics
87 across glacial and interglacial periods. The new record provides a continental perspective of
88 hydroclimate dynamics linked to regional oceanographic conditions.

89

90 **2. Samples and Regional Setting**

91 *2.1 Environmental Setting*

92 We report the analysis of five stalagmites (BG41, BG66, BG67, BG611, BG6LR) from
93 Buraca Gloriosa (BG; 39°32'N, 08°47'W; 420 m a.s.l.) and one stalagmite (GCL6) from Gruta
94 do Casal da Lebre (GCL; 39°18'N, 9°16'W; 130 m a.s.l.), two caves in western Portugal (Fig. 1).
95 Environmental conditions in BG and GCL are well suited for speleothem paleoclimate
96 reconstruction (see below). BG and GCL are located within the Meso-Mediterranean bioclimatic
97 zone that dominates much of Iberia (Fig. 1). This region is characterized by strong seasonality,
98 with warm, dry summers and cool, wet winters (Fig. 2) associated with the winter westerlies
99 (Blanco Castro et al., 1997). In contrast, the Atlantic zone, north of the Douro River, is cooler,
100 wetter, and less strongly seasonal. In the Pleistocene, the transition between these zones likely
101 shifted southward with Mediterranean-type vegetation restricted to refugia (Rey Benayas and
102 Scheiner, 2002).

103 Over interannual scales, the hydroclimate of Iberia is tightly coupled with the winter
104 North Atlantic Oscillation (NAO) (Fig. 3), an atmospheric dipole that strongly influences
105 precipitation across much of western Europe and that more broadly reflects the strength and
106 positioning of the Azores high pressure system, which steers storm tracks contained within the
107 westerlies into or north of Iberia (e.g., Trigo et al, 2002; Paredes et al., 2006; Trouet et al., 2009;

Rhawn Denniston 11/13/2018 4:16 PM
Deleted: 230

Cortesi et al., 2014). The NAO is typically measured as the NAO index, which is calculated using atmospheric pressure differences between Iceland and Lisbon (or the Azores) (Barnston and Livezey, 1987). The nature of the influence of the NAO varies across Iberia, but it is strongly correlated to rainfall in western Portugal (Fig. 3), with a positive NAO index associated with a steeper pressure gradient and elevated Iberian aridity. Iberian precipitation has also been linked to SST in regions ranging from the western North Atlantic to the Iberian margin (Lorenzo et al., 2010) where ocean circulation is dominated by the southward-flowing Portugal Current and the near-coastal, north-flowing Iberian Poleward Current, two systems that transport pollen from river mouths along the continental shelf (Fig. 1).

2.2 Cave Settings

Buraca Gloriosa cave is located near the town of Alvados, 30 km from the Atlantic Ocean, within middle Jurassic limestones of the Estremadura Limestone Massif (Rodrigues and Fonseca, 2010), a topographically distinct region in central Portugal (Fig. 1). The ~35 m-long cave is accessed through a single, small (~0.5 m²) entrance at the top of a collapse at the base of a 30 m-high escarpment (Fig. 4). The cave is well decorated although little active growth is occurring today. Vegetation above the cave is primarily shrubs, small trees, and mosses, hosted by a thin (0-10 cm) and highly organic soil layer.

Gruta do Casal da Lebre overlooks the coastal town of Peniche and is hosted by upper Jurassic limestones. The cave is 130 m long and contains a single, one m² entrance that opens onto a 7 m vertical shaft (Fig. 4). This entrance has been closed with a solid metal door in recent decades in order limit access to the cave, and this modification likely has reduced air exchange in GCL relative to its original state. Like BG, GCL hosts little active calcite deposition, but contains numerous fossil stalagmites and stalactites. The vegetation over the cave has been replaced in recent decades by stands of eucalyptus that grow in thin (<1-5 cm), clay-rich soils.

2.3 Pollen Sources

Pollen deposited on the west Iberian margin is sourced primarily from vegetation inhabiting the watersheds of the major west-flowing stream systems draining Portugal and Spain, which are (from north to south) the Douro, Tagus, and Sado rivers. The areas encompassed by these streams are large (79,000, 81,000, and 7,650 km², respectively) and span a variety of

elevations. The Tagus and Sado are primarily responsible for pollen deposited southwest of Portugal, while the Douro plays an important role in delivering pollen to the more northwesterly sites (Fig. 1). Prevailing wind patterns likely prevent substantial transport of pollen from Iberia to the western Portuguese margin (Naughton et al., 2007). The pollen data presented here were collected in three closely spaced cores from the southwest Iberian margin (MD01-2443: 250-194 ka (Roucoux et al, 2006; Tzedakis et al., 2004); MD01-2444: 193-136 ka (Margari et al., 2010; Margari et al., 2014); MD95-2042: 141-1 ka (Sánchez Goñi et al., 2008; Sánchez Goñi et al., 2013) (Fig. 1) and are integrated here into a single time series.

3. Materials and Methods

3.1 Environmental Monitoring

Environmental conditions were measured at both cave sites over a multi-year period, with data recorded in two-hour intervals near the areas where the stalagmites were deposited. Temperature and relative humidity were obtained using HOBO U23 automated sensors while barometric pressure was recorded with HOBO U20L loggers. Drip rates were monitored at BG with Stalagmate acoustic drip counters (Collister and Matthey, 2008).

3.2 Uranium-Series Dating

Stalagmite chronologies were constructed with a total of 69 ^{230}Th dates obtained at the University of New Mexico (Table 1) using the methods of Asmerom et al. (2010). For dating of stalagmite carbonate, powders ranging from 100-200 mg were transferred into 30 ml Teflon beakers, weighed, dissolved in 15N nitric acid, and then spiked with a mixed ^{229}Th - ^{233}U - ^{236}U tracer and processed using column chemistry methods. U and Th fractions were dissolved in 5 ml of 3% nitric acid and transferred to analysis tubes for measurement on a Thermo Neptune MC-ICP-MS. U and Th solutions were aspirated into the Neptune using a Cetac Aridus II low flow desolvating nebulizer and run as static routines. All isotopes of interest were measured in Faraday cups, except for ^{234}U and ^{230}Th , which were measured in the secondary electron multiplier (SEM). Gains between the SEM and the Faraday cups were determined using standard solutions of NBL-112 for U and an in-house ^{230}Th - ^{229}Th standard for Th that was measured after every fifth sample; chemistry blanks reveal U and Th blanks below 20 pg. Ages are reported using two standard deviation errors.

171 For BG stalagmites, corrections were made for unsupported ^{230}Th using a $^{230}\text{Th}/^{232}\text{Th}$
172 ratio of 13.5 ppm ($\pm 50\%$), a value determined from isotopic analysis of cave dripwater. To
173 obtain this value, 108 ml of dripwater were transferred into six 30 ml Teflon beakers. These
174 beakers were fluxed in 6N HCl for an hour, rinsed, and heated gently on a hotplate until
175 approximately 1-2 ml of fluid remained in each. All solutions were then combined into a single
176 30 ml Teflon beaker, spiked with the same tracer described above (which contains HF), fluxed,
177 and then taken to complete dryness. The resulting precipitate was dissolved with 15N HNO_3 ,
178 dried down, dissolved again in 7N HNO_3 , and processed with the same column chemistry
179 methods used for the stalagmite samples. We lack independent constraints on the initial Th ratio
180 for the GCL stalagmite, and thus apply the default value of 4.4 ppm ($\pm 50\%$). This difference in
181 the initial Th ratio impacts the corrected ages of GCL6 by 0.5-3.0 kyr relative to the value used
182 for BG, and thus does not meaningfully influence our interpretations.

183 Age models were developed via multiple polynomial interpolations between dated
184 intervals using the COPRA age modeling software (Breitenbach et al., 2012) (Fig. 5). Aside from
185 providing age models, COPRA also yields mean modeled stable isotope values and confidence
186 intervals (Supp. Fig. S1). Here we rely primarily here on the original $\delta^{18}\text{O}$ and $\delta^{13}\text{C}$ values
187 because COPRA-derived median values reflect statistically robust variations, but reduce to some
188 degree the range of isotopic variability. For COPRA, a dummy age was included in the age
189 model for BG41 in order to extrapolate below the hiatus, which is only possible with at least two
190 dated points. The value of this dummy age was based on the assumption that it maintains a
191 stratigraphically correct slope (i.e. higher sections of the stalagmite represent younger material).
192 The dummy age was applied a conservative error, meaning that it was as large as possible
193 without causing stratigraphic inversion with respect to the bounding ages.

194

195 3.3 Stable Isotope Ratios

196 A total of 1,510 stable isotope analyses were performed on calcite samples milled from
197 the central axis of each stalagmite. After milling, powders were weighed ($\sim 200\text{ }\mu\text{g}$) and
198 transferred to reaction vessels that were flushed with ultra-pure helium. Samples were then
199 digested using $>100\%$ H_3PO_4 and equilibrated overnight (~ 16 hours) at 34°C before being
200 analyzed. Isotopic ratios were measured using a GasBench II with a CombiPal autosampler
201 coupled to a Thermo Finnigan Delta Plus XL mass spectrometer at Iowa State University. A

combination of internal and external standards was run after every fifth sample, as well as before and after each batch, in order to ensure reproducibility. Oxygen and carbon isotope ratios are presented in parts per mil (‰) relative to the Vienna Pee Dee Belemnite carbonate standard (VPDB). Average precision for both $\delta^{13}\text{C}$ and $\delta^{18}\text{O}$ analyses is better than $\pm 0.1\text{‰}$ (1σ).

For isotopic analyses of soil organic matter and vegetation collected from above the caves, samples were dried, crushed, and transferred to tin boats. Carbon isotopic ratios were measured using a Thermo Finnegan Delta Plus XL mass spectrometer in continuous flow mode coupled with a Costech Elemental Analyzer. Caffeine (IAEA-600), cellulose (IAEA-CH-3), and acetanilide (laboratory standard) isotopic standards yielded an average analytical uncertainty for carbon of $\pm 0.09\text{‰}$ 1σ (VPDB). Dripwater samples were measured using a Picarro L2130-i Isotopic Liquid Water Analyzer, with autosampler and ChemCorrect software. Each sample was measured six times, with only the last three injections used to determine isotopic values in order to minimize memory effects. Three reference standards (VSMOW, IAEA-OH-2, IAEA-OH-3) were used for regression-based isotopic corrections and to assign the data to the appropriate isotopic scale. Reference standards were measured at least once every five samples. The average analytical uncertainty for $\delta^{18}\text{O}$ measurements was $\pm 0.1\text{‰}$ 1σ (VSMOW).

3.4 Stalagmite Mineralogy and Fabrics

The calcite comprising the BG samples ranges across a variety of fabrics including a faster-growing, white, fibrous form and a slower-growing, dense, clear structure (Fig. 6; Supp. Fig. S2). In samples, sharp changes between the two forms within the same growth horizons mark intervals of recrystallization during which U/Th ages are highly inconsistent, and these intervals were excluded from our data set. BG6LR, which grew discontinuously over much of the last glacial cycle, suffered from alteration of early and middle Holocene material, which was therefore excluded from this analysis. BG67 is characterized primarily by fibrous calcite that has been recrystallized to clear, dense calcite in a narrow band descending through its core. U/Th dates from the fibrous calcite on the margins of the growth surface reveal open system behavior and thus this portion of BG67 was excluded. Recrystallization is evident in portions of GCL6 (particularly just above its base) and BG66 but the consistency of U/Th dates and the trends in stable isotopes suggest that this alteration may have occurred soon after original deposition. We tested whether these altered sections retain reliable paleoclimatic information by analyzing stable

isotopes along partial transects located just outside the zones of recrystallization (Fig. 6). Because stable isotopic values and trends between these transects were consistent (within the analytical errors), we retained these sections in the time series. Growth position changed at numerous times in several of these stalagmites, and our sampling strategy accounted for these changes so as to consistently collect samples for stable isotopic analysis from the top surface (cap) of each stalagmite rather than the margins.

4. Results

4.1 Environmental Monitoring

Temperature and relative humidity collected inside both caves document environmental conditions over a multi-year period. Relative humidity remained largely stable at ~100% in both caves. Temperatures, while different at the two sites, exhibited similar seasonal variability that approximates the mean average temperature of the region ($14.2 \pm 0.4^\circ\text{C}$ at BG and $16.2 \pm 0.3^\circ\text{C}$ at GCL for August 2012-January 2018) (Fig. 7).

Dripwater was collected at BG both over the course of minutes during site visits on four separate occasions (November 2014, October 2015, March 2016, January 2018) and as months-long integrated samples. A total of 25 dripwater samples were analyzed for stable isotopic values. Dripwater $\delta^{18}\text{O}$ values range from -2.4‰ to -4.6‰, with a mean of $-3.8 \pm 0.8\text{‰}$ (Supp Table 1), although as the timing of site visits varied, this value clearly is impacted by seasonal controls on precipitation (and thus infiltration) oxygen isotope values. Drip rates were measured for much of the period spanning June 2014 to January 2018 (for a total of ~36 months) and exhibit seasonal variations tied to the winter wet and summer dry seasons, as well as individual rain events (Fig. 7).

4.2 U-Th Dates and Age Models

^{234}U - ^{230}Th dating of BG and GCL stalagmites reveals growth across approximately three quarters of the last 220 ka, with periods of deposition interrupted by numerous hiatuses of varying length, with the longest gaps from 160-147, 97-87, 72-60, 41-36, 32-30, and 17-15 ka (Fig. 5 and 6; Supp. Fig. S3). These features, coupled with repeated changes in growth direction and high ^{232}Th abundances in select sections, complicate construction of a chronology in some intervals. Macroscopic petrographic discontinuities suggest the presence of several short-lived

Rhawn Denniston 11/13/2018 4:16 PM
Deleted: 230

hiatuses, but these were included as gaps in the age models only where U/Th dates reveal an identifiable temporal offset. For example, the marine isotope stage (MIS) 6/5e boundary recorded by stalagmite BG67 is marked by both a change in drip position and a sharp transition from dense, clear calcite to a white, fibrous form. Taken together, it is clear that a hiatus of some duration occurred at this time. However, these isotope data are presented as being uninterrupted given the continuity of $\delta^{18}\text{O}$ values and no U/Th evidence for a long-lived hiatus (Fig. 6).

271

272 4.3 Assessing *Equilibrium* in Speleothem $\delta^{18}\text{O}$ and $\delta^{13}\text{C}$ Values

273 We used two approaches to assess the fidelity of BG/GCL carbon and oxygen isotopes as
274 records of past environmental variability. First, Hendy Tests, in which stalagmite isotopic ratios
275 must satisfy two criteria in order to be considered as having crystallized near isotopic
276 equilibrium with cave dripwater (Hendy, 1971), were performed for each stalagmite. The first
277 half of the Hendy Test involves analysis of multiple isotopic analyses performed on samples
278 drilled at increasing distance from the central growth axis along the same series of growth layers.
279 The conceptual justification for this approach is that dripwater, and thus speleothem calcite, $\delta^{18}\text{O}$
280 values should remain constant down the stalagmite flanks because ^{16}O preferentially lost to CO_2
281 out-gassing is replenished by CO_2 hydration and hydroxylation reactions. Progressive ^{18}O
282 enrichment associated with kinetic effects tied to Rayleigh distillation suggests isotopic
283 disequilibrium. No such consistent trends toward elevated oxygen isotopic ratios are found (Fig.
284 8), and thus the BG/GCL stalagmites appear to satisfy the first criterion of the Hendy Test.

285 The second portion of the Hendy Test is based on the degree of covariation of carbon and
286 oxygen isotopic ratios. Oxygen isotopic ratios of speleothem calcite reflect those of infiltrating
287 fluids, which are generally close to the $\delta^{18}\text{O}$ values of meteoric precipitation, and which, in many
288 locations, are linked to climate (air temperature, moisture source, seasonality of precipitation, or
289 rainfall amount, (Lachniet, 2009)). Interpreting changes in oxygen isotope composition at
290 BG/GCL during intervals of profound climatic change such as marked the last glacial period is
291 complicated by the multiple factors that influenced $\delta^{18}\text{O}$ values of precipitation at these sites,
292 including shifts in moisture source. The potential exists for rainfall in Iberia to be derived from
293 atmospheric moisture sources that change on synoptic/seasonal scales (Moreno et al., 2014;
294 Gimeno et al., 2010; Gimeno et al., 2012) as well as in response to changing glacial boundary
295 conditions (Florineth and Schlüchter, 2000; Kuhlemann et al., 2008; Luetscher et al., 2016). In

Rhawn Denniston 11/13/2018 4:16 PM

Deleted: Environmental Signals

Rhawn Denniston 11/13/2018 4:16 PM

Deleted: Isotopic Ratios

Rhawn Denniston 11/13/2018 4:16 PM

Deleted:). Oxygen isotopic ratios in stalagmites primarily reflect the $\delta^{18}\text{O}$ value of effective precipitation, as only an extremely small proportion of oxygen in dripwater is contributed by dissolution of CO_2 or bedrock carbonate (Lachniet, 2009).

304 addition, strong but opposite correlations exist in modern precipitation between rainwater $\delta^{18}\text{O}$
305 values and (i) the regional air temperature ($r=+0.8$) and (ii) rainfall amount ($r=-0.8$), both of
306 which are related to the strong seasonality of precipitation associated with Meso-Mediterranean
307 climates (IPMA, 2016).

308 Correlations between carbon and oxygen isotope ratios are presented in Figure 8. Three
309 stalagmites – BG6LR, BG66, and BG67 – show strong correlations between $\delta^{13}\text{C}$ and $\delta^{18}\text{O}$
310 ($r^2=0.6$), while the other three samples lack a strong correlation. If one considers the second
311 criterion of the Hendy Test, the nature of equilibrium crystallization in stalagmites BG6LR,
312 BG66, and BG67 would be considered suspect. It must be noted, however, that the reliability of
313 the Hendy Test has been questioned because (1) equilibrium may be maintained in some portions
314 of a stalagmite but not others, (2) growth layers thin progressively down the sides of the
315 stalagmite, making it difficult to restrict samples to the same material, and (3) equilibrium
316 covariation of carbon and oxygen isotope ratios may result as the direct or indirect result of
317 climatic variability (Dorale and Liu, 2009; Lechleitner et al., 2017). We therefore interpret both
318 isotope ratios and their covariation as environmental signals.

Rhawn Denniston 11/13/2018 4:16 PM
Moved (insertion) [1]

320 4.4 Hydroclimate Proxies

321 4.4.1 Carbon Isotopes

322 Interpreting speleothem $\delta^{13}\text{C}$ variability in a climatic context requires understanding, or
323 at least constraining, the origins of these isotopic shifts. Stalagmite $\delta^{13}\text{C}$ values reflect two
324 primary inputs: CO_2 derived from the atmosphere and/or soil zone and bicarbonate derived from
325 dissolution of bedrock carbonate. Speleothem $\delta^{13}\text{C}$ values reflect the type (C_3 vs C_4) and density
326 of vegetation over the cave, both of which are impacted by changes in air temperature and/or
327 precipitation. The average $\delta^{13}\text{C}$ value of biogenic CO_2 in the soil zone is tied to the ratio of
328 plants utilizing the C_3 (average $\delta^{13}\text{C}$ -26‰) versus C_4 (average $\delta^{13}\text{C}$ -14‰) photosynthetic
329 pathways (Deines, 1980; von Fischer et al., 2008). Similarly, vegetation density and soil
330 respiration rates over the cave impact the relative contribution of atmospheric CO_2 (pre-
331 Industrial $\delta^{13}\text{C}$ -6‰ to -7‰; Francey et al., 1999) as compared to soil-derived CO_2 (Hellstrom
332 and McCulloch, 2000; Genty et al., 2003). Phanerozoic bedrock $\delta^{13}\text{C}$ values range from -4‰ to
333 +8‰ (Saltzman and Thomas, 2012), but these values are static and do not contribute to temporal
334 variability in stalagmite carbon isotopic ratios.

Rhawn Denniston 11/13/2018 4:16 PM
Moved (insertion) [2]

335 Superimposed on these inputs are secondary effects capable of influencing the $\delta^{13}\text{C}$
 336 values of dripwater in the epikarst or cave. When voids in the bedrock are not fully saturated,
 337 CO_2 degassing from infiltrated water may occur in the epikarst. This preferential loss of $^{12}\text{CO}_2$
 338 (that may result in crystallization of calcium carbonate – so-called prior calcite precipitation)
 339 enriches the residual solution in ^{13}C , a signal that can be transferred into underlying stalagmites
 340 (Baker et al., 1997). Once the solution enters the cave, equilibrium fractionation between
 341 dissolved carbon species may be disrupted owing to issues surrounding CO_2 -degassing under
 342 low drip rate conditions (Breitenbach et al., 2015) or by disequilibrium processes occurring
 343 during carbonate crystallization (Mickler et al., 2004; Fairchild et al., 2006). Importantly, $\delta^{13}\text{C}$
 344 values reflect local infiltration rather than (pan-)regional atmospheric conditions as in the case of
 345 $\delta^{18}\text{O}$. This difference between both proxies offers the opportunity to investigate environmental
 346 changes at different spatial scales.

347
 348
 349
 350
 351
 352
 353
 354
 355
 356
 357
 358

359 Terrestrial deposits preserving pollen spectra spanning substantial portions of the last
 360 glacial cycle from western Iberia are rare (Gómez-Orellana et al., 2008; Fletcher et al., 2010;
 361 Moreno et al., 2012), and thus pollen in marine sediments represents a particularly important
 362 continental climate record. Pollen samples obtained from the Iberian margin contain small
 363 percentages of *Poaceae*, the family including the majority of C_4 plants, demonstrating a
 364 persistent and overwhelming majority of C_3 (largely shrub and arboreal) vegetation throughout
 365 the last glacial cycle including between Greenland stadials (GS) and interstadials (GI) and across

Rhawn Denniston 11/13/2018 4:16 PM

Moved up [1]: Correlations between carbon and oxygen isotope ratios are presented in Figure 8. Three stalagmites – BG6LR, BG66, and BG67 – show strong correlations between $\delta^{13}\text{C}$ and $\delta^{18}\text{O}$ ($r^2=0.6$), while the other three samples lack a strong correlation. If one considers the second criterion of the Hendy Test, the nature of equilibrium crystallization in stalagmites BG6LR, BG66, and BG67 would be considered suspect. It must be noted, however, that the reliability of the Hendy Test has been questioned because (1) equilibrium may be maintained in some portions of a stalagmite but not others, (2) growth layers thin progressively down the sides of the stalagmite, making it difficult to restrict samples to the same material, and (3) equilibrium covariation of carbon and oxygen isotope ratios may result as the direct or indirect result of climatic variability (D... [1])

Rhawn Denniston 11/13/2018 4:16 PM

Moved down [3]: test of equilibrium crystallization in the modern system can be constructed by comparing modeled stalagmite isotopic values to recently deposited calcite. The carbon isotopic composition of speleothem calcite is the result of a com... [3]

Rhawn Denniston 11/13/2018 4:16 PM

Deleted: ... [2]

Rhawn Denniston 11/13/2018 4:16 PM

Deleted: This approach, while certainly overly simplified for the BG system, yields modeled stalagmite $\delta^{13}\text{C}$ values of $-7.7\pm 1\%$, similar to calcite crystallized on two glass slides installed at the site of two active... [4]

Rhawn Denniston 11/13/2018 4:16 PM

Moved down [4]: value of $-3.1\pm 1.0\%$ is nearly identical to the glass plate-grown calcite value of $-3.0\pm 0.6\%$. It should be noted, however, that assessing equilibrium crystallization in modern calcite/dripwater pairs at BG is complicated by the low t... [5]

Rhawn Denniston 11/13/2018 4:16 PM

Deleted: 230 ka (Fig.

Rhawn Denniston 11/13/2018 4:16 PM

Moved down [5]: 9), although stalagmites spanning the same periods of time are restricted to 187-185, 111-104, 83-81, 78-73, and 58-53 ka. Because these intervals are short, and because the temporal resolution varies substantially between stalagmites... [6]

Rhawn Denniston 11/13/2018 4:16 PM

Moved up [2]: ...
 4.4 Hydroclimate Proxies ...
 4.4.1 Carbon Isotopes ...
 Interpreting speleothem $\delta^{13}\text{C}$ variability in a climatic context requires understanding... [7]

Heinrich stadials (HS) (d'Errico and Sánchez Goñi, 2003; Tzedakis et al., 2004; Desprat et al., 2006; Sánchez Goñi et al., 2008; Sánchez Goñi et al., 2013; Margari et al., 2014). In the absence of changes in vegetation type, shifts in the source of carbon found in cave dripwater therefore likely originated with the density of vegetation and/or soil respiration rates (Genty et al., 2003). Reductions in these values are generally associated with decreases in temperature and/or increases in aridity, such as have been inferred from Iberian pollen spectra to have characterized Iberia during GS, HS, and glacial maxima (Sánchez Goñi et al., 2008; Margari et al., 2014). Complementing these effects are increases in the contribution of bedrock carbon, as well as prior calcite precipitation, reflecting a combination of longer residence times of infiltrating solutions and desaturation of voids in the epikarst above the cave, both of which are consistent with more arid climates (Baker et al., 1997; Genty et al., 2003). Thus, we interpret the carbon isotopic values of the BG/GCL record as primarily a local (hydro)climate proxy, with higher $\delta^{13}\text{C}$ values indicative of a cooler, drier climate. Integrating the GCL6 $\delta^{13}\text{C}$ record into the BG time series is complicated by the slightly different bedrock $\delta^{13}\text{C}$ values of the host rocks (Supp. Table 1) and what may have been distinct vegetation types and cave hydrologies at each cave when GCL6 was being deposited (187-160 ka). However, similar $\delta^{13}\text{C}$ values during their period of overlap (187-185 ka) suggests that the two records can be consolidated (see below).

A test of equilibrium crystallization in the modern system can be constructed by comparing modeled stalagmite isotopic values to recently deposited calcite. The carbon isotopic composition of speleothem calcite is the result of a complex series of reactions that have been addressed in a number of studies (Hendy, 1971; Mühlinghaus et al., 2007; Dreybott, 2008). For $\delta^{13}\text{C}$ in BG stalagmites, we use the equations of Li et al. (2014), which factor in the two primary sources of carbon – soil CO_2 and bedrock carbonate – the proportion of carbon derived from each source, and temperature-induced fractionation of carbon isotopes between dissolved carbon species:

$$\delta^{13}\text{C}_{\text{calcite}} = f_l * [\delta^{13}\text{C}_l - (\delta^{13}\text{C}_{\text{CO}_2(\text{g})} + 9.48 \times 10^3 / T - 23.89)] + \delta^{13}\text{C}_{\text{CO}_2(\text{g})} + 9.48 \times 10^3 / T + 0.049T - 37.72$$

where: f_l = fraction of bicarbonate from limestone (ls)

T = temperature ($^{\circ}\text{K}$)

Rhawn Denniston 11/13/2018 4:16 PM

Deleted: as previously discussed, the

Rhawn Denniston 11/13/2018 4:16 PM

Deleted: .

Rhawn Denniston 11/13/2018 4:16 PM

Moved (insertion) [3]

We assume the most straightforward and simple situation: the system remains closed to soil CO₂ and bedrock carbonate contributes 50% of carbon to dripwater bicarbonate ($f_i=0.5$). We apply the average cave temperature of 14.4°C and the measured $\delta^{13}\text{C}$ values of BG bedrock and the overlying vegetation/soil of $+3\pm 1\text{‰}$ and $-28\pm 1\text{‰}$, respectively. This approach, while certainly overly simplified for the BG cave system, yields modeled stalagmite $\delta^{13}\text{C}$ values averaging $-7.7\pm 1\text{‰}$, similar to calcite crystallized on two glass slides installed at the site of two actively growing stalagmites in the loft area of BG, which yielded $\delta^{13}\text{C}$ values of $-8.4\pm 1.2\text{‰}$.

4.4.2 Oxygen Isotopes

The origins of BG/GCL isotopic variability appear more complex for oxygen than for carbon. Like $\delta^{13}\text{C}$ values, local $\delta^{18}\text{O}$ minima mark interstadials and interglacials. Analysis of modern precipitation data reveals equally strong, albeit inverse, correlations between precipitation $\delta^{18}\text{O}$ and both amount ($r=-0.8$) and air temperature ($r=+0.8$) effects, likely owing to the dominance of cool season precipitation in annual water budgets (IAEA/WMO, 2016) (Fig. 2). Based on these relationships, it remains possible that changes in air temperature, overall precipitation, and/or precipitation seasonality could impact the $\delta^{18}\text{O}$ values of effective moisture. That air temperature is likely not a prominent driver of stalagmite oxygen isotopic variability is supported by two observations, however. First, the slopes of the air temperature/ $\delta^{18}\text{O}$ relationships ($\text{‰}/^\circ\text{C}$) at the three GNIP stations located closest to BG and GCL (Porto, Vila Real, and Portalegre) are nearly identical (average for the three sites of $0.25\pm 0.03\text{‰}/^\circ\text{C}$) but opposite in sign, to the calcite-water temperature dependence of oxygen isotopic fractionation ($-0.2\text{‰}/^\circ\text{C}$) (Kim and O'Neil, 1997) (slopes of precipitation amount/ $\delta^{18}\text{O}$ are -1.6 , -3.5 , and $-3.7\text{‰}/100\text{ mm/month}$, respectively). In the simplest sense, therefore, a 1°C increase in mean annual air temperature (and thus also cave temperature) would increase precipitation $\delta^{18}\text{O}$ values by approximately the same amount that the water temperature effect would lower stalagmite calcite $\delta^{18}\text{O}$ values. In this simplified scenario, the net effect is a stalagmite record that is negligibly influenced by multi-decadal/centennial-scale temperature changes alone. Secondly, the observed shift toward lower stalagmite $\delta^{18}\text{O}$ values during interstadials and interglacials, periods of elevated mean annual temperature, demonstrates that the observed positive correlation between precipitation $\delta^{18}\text{O}$ and air temperature is not a dominant feature over millennial time scales. For

Rhawn Denniston 11/13/2018 4:16 PM

Deleted:),

Rhawn Denniston 11/13/2018 4:16 PM

Deleted:),

568 example, the 3.5‰ decrease in $\delta^{18}\text{O}$ values between MIS 6 and MIS 5e (136-128 ka) (Fig. 9) can
569 be only partially accounted for by the ~1‰ ice volume-related decrease in North Atlantic surface
570 water $\delta^{18}\text{O}$ values (Schrag et al., 1996). Other factors such as kinetics associated with humidity
571 and wind speed at the point of evaporation (Grootes et al., 1993), temperature and source of
572 atmospheric moisture (Herbert et al., 2001), and cloud evolutionary pathways (Rozanski and
573 Araguás, 1995) need also be considered but cannot account for the entirety of this shift. Because
574 of the narrow continental shelf in central Portugal, the LGM shoreline was located close to the
575 modern shoreline, thereby minimizing continental effects, and the magnitude of the impacts of
576 wind speed and ocean temperature do not appear sufficient to account for the observed
577 stalagmite $\delta^{18}\text{O}$ variability. Thus, the decrease in stalagmite $\delta^{18}\text{O}$ between the penultimate glacial
578 and last interglacial suggests that stalagmite oxygen isotope ratios are primarily recording (pan-
579)regional hydroclimate rather than temperature. The origin of the anomalously low $\delta^{18}\text{O}$ values
580 during GI 1 (dated here from 14.5-13.9 ka) are unclear (unfortunately no other BG or GCL
581 stalagmite also spans this interval) but reinforce this inverse relationship between mean annual
582 temperature and stalagmite oxygen isotope ratios.

583 Speleothem oxygen isotopic ratios were modeled using the paleotemperature equation of
584 Kim and O'Neil (1997), which requires measurements of cave temperature and dripwater $\delta^{18}\text{O}$
585 values. The resulting $\delta^{18}\text{O}$ model value of $-3.1 \pm 1.0\text{‰}$ is nearly identical to the glass plate-grown
586 calcite value of $-3.0 \pm 0.6\text{‰}$. It should be noted, however, that assessing equilibrium
587 crystallization in modern calcite/dripwater pairs at BG is complicated by the low temporal
588 resolution associated with integrated, months-long dripwater samples, variable timing of
589 dripwater collecting trips, and any seasonal biases in calcite crystallization that at present remain
590 poorly constrained.

591 Replication between stalagmites of similar age is arguably the single most reliable
592 method for evaluating the impacts of climate versus secondary influences, including evaporation
593 and kinetic effects (Denniston et al., 1999; Mickler et al., 2004), on stalagmite isotopic ratios
594 (Dorale and Liu, 2009; Denniston et al., 2013). When presented as an integrated data set, the
595 BG/GCL stalagmite carbon and oxygen isotopic time series spans the majority of the last 220 ka
596 (Fig. 9), although stalagmites spanning the same periods of time are restricted to 187-185, 111-
597 104, 83-81, 78-73, and 58-53 ka. Because these intervals are short, and because the temporal
598 resolution varies substantially between stalagmites, replication tests based on these intervals are

Rhawn Denniston 11/13/2018 4:16 PM
Moved (insertion) [4]

Rhawn Denniston 11/13/2018 4:16 PM
Moved (insertion) [5]

of limited utility. However, within the age uncertainties, $\delta^{18}\text{O}$ and $\delta^{13}\text{C}$ values and trends are similar, suggesting that oxygen and carbon isotopic ratios track environmental, rather than drip-specific, variables. The three exceptions in which coeval samples do not replicate well are: $\delta^{13}\text{C}$ values offset by 3‰ from 83-81 ka and by 4‰ from 58-53 ka, and $\delta^{18}\text{O}$ values offset by 1‰ from 111-104 ka (Fig. 9; Supp. Fig. S4).

4.4.3 $\delta^{234}\text{U}$ Values

$\delta^{234}\text{U}$ values (calculated as the difference between the age-corrected $^{234}\text{U}/^{238}\text{U}$ ratio of a sample and the secular equilibrium $^{234}\text{U}/^{238}\text{U}$ ratio) of speleothem carbonate have also been used as a proxy for paleoprecipitation (Hellstrom and McCulloch, 2000; Oster et al., 2012; Plagnes et al., 2002; Polyak et al., 2012; Zhou et al., 2005). ^{234}U exists in the stalagmite crystalline lattice due to incorporation from cave dripwater and through *in situ* production from decay of ^{238}U . Alpha recoil displaces ^{234}U from its lattice position, increasing its susceptibility to leaching by infiltrating waters, meaning that ^{234}U is selectively mobilized relative to ^{238}U in cave dripwater (Chabaux et al., 2003; Oster et al., 2012). The flux of infiltrating fluids is therefore tied to $\delta^{234}\text{U}$ values of dripwater, and thus stalagmite carbonate, such that decreases in effective precipitation and/or bedrock dissolution rate, both of which are tied to increased aridity, are associated with elevated speleothem $\delta^{234}\text{U}$ values (Hellstrom and McCulloch, 2000; Plagnes et al., 2002; Polyak et al., 2012).

As differences in $\delta^{234}\text{U}$ values between stalagmites may arise from distinct infiltration pathways (Zhou et al., 2005), complicating the integration of $\delta^{234}\text{U}$ values from multiple stalagmites into a single, cohesive data set, we restrict our analysis to stalagmite BG6LR, which represents the longest individual stalagmite record of the BG/GCL time series. While the number of $\delta^{234}\text{U}$ measurements is small compared to stable isotopic values, the temporal density of the former is sufficient to demonstrate the utility of $\delta^{13}\text{C}$ and $\delta^{18}\text{O}$ values as paleohydroclimate proxies (Fig. 9). Decreased precipitation/effective moisture is associated with elevated stalagmite $\delta^{13}\text{C}$, $\delta^{18}\text{O}$, and $\delta^{234}\text{U}$ values. The relationships between $\delta^{13}\text{C}$ and $\delta^{234}\text{U}$ values in all BG and GCL stalagmites are presented in Supp. Fig. S5.

5. Environmental Conditions at BG/GCL and Links to Iberian Margin SST

The previously discussed tests for isotopic equilibrium, including the reproducibility of carbon and oxygen isotope ratios between coeval BG and GCL stalagmites, support the notion that their $\delta^{13}\text{C}$ and $\delta^{18}\text{O}$ values may be integrated into cohesive time series reflecting paleohydroclimatic conditions and used to assess links between continental climate and SST (Fig. 10). Over the last several glacial cycles, oceanographic conditions along the western Iberian margin varied at millennial and orbital time scales in close correlation with Greenland air temperature and North Atlantic conditions and circulation (Roucoux et al., 2005; Danialu et al., 2007; Sánchez Goñi et al., 2008; Darfeuil et al., 2016). Abrupt changes in SST reflect a balance between southward expansion of subpolar waters and northward migration of subtropical water masses (de Abreu et al., 2003). During the particularly cold conditions characterizing HS and GS, Iberian margin SST decreased by up to 9°C (to as much as 13°C below present values; de Abreu et al., 2003), with these changes helping to position the arctic or subarctic front at ~39°N, the same latitude as BG and GCL. These cold surface waters reduced the production and transport of atmospheric moisture to Iberia (Eynaud et al., 2009; Voelker and de Abreu, 2011), and would have thereby influenced the timing of speleothem growth and carbon and oxygen isotopic values in BG and GCL stalagmites. Indeed, the composite BG/GCL record documents coherence, at both orbital and millennial scales, between Portuguese hydroclimate, vegetation, and Iberian margin SST during the last two glacial cycles (Fig. 10 and 11). In an attempt to quantify this covariance, we binned the SST and stalagmite stable isotope data into century-long intervals. The relatively short record of BG41 was not included, and model ages for stalagmites BG66 and GLC6 were increased by 4.0 kyr and 1.3 kyr, respectively, to improve correlation with the SST chronology. The resulting inverse correlation between SST and carbon and oxygen is strong ($r=-0.55$ and -0.52 , respectively; $p<0.0001$) (Supp. Fig. S6).

5.1 Growth Intervals

The single most fundamental prerequisite to speleothem deposition is infiltration of surface waters, and thus the timing of stalagmite growth can reflect changes in mean hydroclimatic state. Deposition of multiple BG stalagmites was punctuated by hiatuses spanning similar time intervals (although the precise ages of the onset and/or termination of the hiatuses are distinct), a relationship that suggests links to changes in hydroclimate rather than random drip site-specific variability.

660 Hiatuses in some BG samples coincide with HS1, HS3, HS4, and HS6, and pollen spectra
661 independently suggest increased aridity during HS and glacial maxima. Decreases in arboreal
662 pollen abundance and concomitant increases in drought-tolerant vegetation coincide with periods
663 of reduced SST. Vegetation patterns during maximal IRD deposition on the Iberian margin
664 reveal not only dramatically reduced forest cover but also a pronounced expansion of semi-desert
665 plants (e.g. Sánchez Goñi et al., 2000; Roucoux et al., 2005; Naughton et al., 2009). These
666 changes mark the long hiatus between HS7 and HS6 (71-59 ka), which overlaps with the some of
667 the coldest SST of the last 70 ka as reconstructed using U_{37}^k at core MD95-2042 (Darfeuil et al.,
668 2016) (Fig. 10; Fig. 12). An absence in BG stalagmite deposition from ~160-149 ka occurs at the
669 same time as massive seasonal discharges from the Fleuve Manche river and the coldest
670 continental climates and SST (157-154 ka) of the last 220 ka, as determined from pollen and
671 foraminifera from core MD01-2444 (Margari et al., 2014; Fig. 1).

672 Whether hiatuses in BG speleothem deposition are a result of pronounced reductions in
673 precipitation, an extension of below freezing temperatures that limited infiltration (Vaks et al.,
674 2013; Fankhauser et al., 2016), or variations in infiltration pathway/drip position is ambiguous.
675 Pollen transfer functions from MD95-2042 suggest winter temperatures dropped below 0°C
676 during HS and annual precipitation was reduced by up to 50% (from 800 mm to 500-400 mm
677 during HS3, HS4, and HS5) (Sánchez Goñi et al., 2002). Applying this temperature
678 reconstruction to western Portugal is complicated, however, by the broad area across which these
679 pollen were sourced. Permafrost reconstructions (Vandenberghe et al., 2014) of Iberia argue
680 against the hypothesis that continuous sub-zero temperatures inhibited infiltration and stalagmite
681 growth. We thus suggest that the hiatuses observed at BG and GCL were driven largely by
682 reductions in precipitation.

683 Other western European cave records also share similar growth histories. For example,
684 stalagmites from Villars Cave, southwestern France (Genty et al., 2003; Genty et al., 2010;
685 Wainer et al., 2011), and from multiple caves in northern Spain (Stoll et al., 2013) (Fig. 1) are
686 also punctuated by hiatuses during HS. For example, at or near HS7, stalagmite hiatuses were
687 formed at Villars Cave (78-76 ka), in northern Spain (~75 k), and BG (80-78 ka). No stalagmite
688 deposition has been identified at BG from 71-60 ka or Villars cave from 67-62 ka, a period that
689 includes HS6. Finally, HS1 is marked by a hiatus in northern Spain (18-15.5 ka) and at BG (17-
690 15 ka). While the timing of these hiatuses is not identical, and not all hiatuses at Villars Cave and

Rhawn Denniston 11/13/2018 4:16 PM
Deleted: 230

692 the Spanish caves are coincident with those at BG, the substantial degree of overlap suggests a
693 common origin. Stoll et al. (2013) noted that stalagmite deposition and/or elevated growth rates
694 in northern Spain stalagmites occurred during periods of high Northern Hemisphere summer
695 insolation or during GI, while hiatuses occurred during periods of low insolation and low SST
696 ($<13.7^{\circ}\text{C}$). The BG record supports the hypothesis that growth interruptions are related to SST
697 controls on regional atmospheric moisture availability, although the impact of insolation is not
698 clear.

699

700 5.2 BG/GCL Stable Isotopic and $\delta^{234}\text{U}$ Variability

701 Stalagmite $\delta^{13}\text{C}$ and $\delta^{18}\text{O}$ values covary with changes in SST at orbital time scales. The
702 offset between interglacial and glacial isotopic values averages $\sim 3\text{‰}$ for $\delta^{18}\text{O}$ and $\sim 7\text{‰}$ for $\delta^{13}\text{C}$
703 values (Fig. 10). Stalagmite $\delta^{234}\text{U}$ values also preserve these changes in aridity. Millennial-scale
704 changes are also recorded in stalagmite carbon isotope ratios, with shifts of 3-7‰ associated
705 with GI/GS transitions, and oxygen isotopic changes of $\sim 1\text{--}2\text{‰}$. The large swing in $\delta^{18}\text{O}$ values
706 during the transition from GI-1 to the Younger Dryas (YD) ($\sim 5\text{‰}$ from 14.0-13.5 ka) is
707 anomalous. Given that the change in $\delta^{13}\text{C}$ values at this time (6‰) is consistent with other GI
708 transitions, the hydroclimatic implications of this interval require additional study. Similarly,
709 oxygen and carbon isotopic variability is pronounced during the late Holocene portion of the BG
710 record. The origin of this high variability is unclear. Replication of the Holocene portion of this
711 record currently underway will help address this question (Thatcher et al., 2018).

712 Where growth is continuous during HS, the link between stalagmite isotopic variations
713 and SST changes is clearly visible (Fig. 11). Prominent positive carbon isotopic excursions
714 define the YD, HS2, HS5, HS6, and HS8, consistent with diminished concentrations of arboreal
715 pollen in cores from the Iberian margin, and serve to document particularly cold and dry
716 conditions at these times (Sánchez Goñi et al., 2000; Roucoux et al., 2006; Sánchez Goñi et al.,
717 2008). Reduced stalagmite $\delta^{13}\text{C}$ values mark periods of enhanced effective moisture from 170-
718 160 and 145-135 ka, tracking peaks in temperate tree pollen and alkenone-based SST. The BG
719 record reveals a pronounced increase in stalagmite $\delta^{13}\text{C}$ values during the YD, at odds with the
720 plateau in SST observed in some Portuguese coastal margin sediments at this time. However, a
721 higher resolution SST record reveals a pronounced drop in SST (Rodrigues et al., 2010), well
722 matched with the BG isotopic profile and the stalagmite record from Villars Cave.

723 Hydroclimatic shifts associated with GS and GI are most clearly expressed during MIS
724 5a and 5b in the BG carbon isotope record (Fig. 11). Other European stalagmite records have
725 identified GI/GS events from the last glacial period (Genty et al., 2003; Spötl et al., 2006; Boch
726 et al., 2011; Moseley et al., 2014) (Fig. 10), but the level of resolution recorded in the BG/GCL
727 time series has not been clearly identified previously in western Iberia. A carbon isotope time
728 series (albeit with low temporal resolution) of a flowstone from southeastern Spain does not
729 present clear evidence of either GI or most HS during the last glacial cycle, although it does
730 contain a clear expression of HS11 (Hodge et al., 2008) (Fig. 1). And while some Iberian lakes
731 and peat bogs document environmental changes concurrent with HS, no single record, including
732 one of the longest - the 50 ka time series from the Fuentillejo maar, south-central Spain -
733 contains a consistent signal for all HS (Vegas et al., 2010; Moreno et al., 2012) (Fig. 1). GS/GI
734 oscillations during MIS 3 are not clearly defined in BG stalagmites, likely owing to insufficient
735 temporal resolution, although the BG records does share a resemblance to reconstructed SST
736 variability (Fig. 11).

737 Whether the apparent inconsistent linkages between Iberian margin SST and Iberian
738 hydroclimate are due to the limitations of these proxies, region-specific responses to SST
739 variations, or a changing influence of SST on precipitation is unclear. However, other points of
740 divergence between SST and the BG/GCL records exist. For example, some marine cores reveal
741 a prominent spike in forest taxa occurring at the start of interglacials, decreasing thereafter for
742 the next 5-10 kyr (Tzedakis et al., 2004; Desprat et al., 2007) (Fig. 10). This early interglacial
743 peak is a common feature in several time series including the Antarctic δD (Petit et al., 1999)
744 and CH_4 records (Louergue et al., 2008), and in stalagmite isotopic ratios from the eastern
745 Mediterranean (Bar-Matthews et al., 2003) and southern France (Couchoud et al., 2009) (Fig.
746 10). The BG/GCL $\delta^{13}C$ and $\delta^{18}O$ records lack this feature, although the previously discussed
747 issues surrounding the continuity of the MIS6/5e transition may complicate identifying it.

748 Stalagmite $\delta^{13}C$ and $\delta^{18}O$ values are lower during GI 20-22 (MIS 5a/4; 84-72 ka) than in
749 either the Holocene or MIS 5e (Fig. 10 and 12), and BG6LR $\delta^{234}U$ values support this
750 observation. This interval is of particular interest given that Atlantic forest pollen, which has
751 been used as a proxy for air temperature, was decoupled from SST across northwestern Iberia
752 during cold events (C18-C20) (Rousseau et al., 2006; Rasmussen et al., 2014). This decoupling
753 is interpreted as reflective of a weakened control of SST on Iberian atmospheric temperature

that, in turn, enhanced transport of atmospheric vapor to the high latitudes, amplifying production of ice sheets in the early stages of the last glacial cycle (Sánchez Goñi et al., 2013). This process has also been demonstrated for an earlier interglacial (MIS 19; Sánchez Goñi et al., 2016). Other offsets include (1) the gradual change in BG $\delta^{13}\text{C}$ and $\delta^{18}\text{O}$ values across the MIS 8/7 boundary, in contrast to the sharp rise in SST at this time; (2) the anomalously large $\delta^{13}\text{C}$ response to ice rafting event C24 (111-108 ka), and (3) the persistence of low $\delta^{13}\text{C}$ values as SST decreased from 205-187 ka (Fig. 11 and 12).

The mechanism linking SST and Iberian hydroclimate over millennial time scales remains unclear. The NAO exerts a strong control over Iberian precipitation, and previous studies have suggested that GS and GI (Moreno et al., 2002; Sánchez Goñi et al., 2002; Danianu et al., 2007) and HS (Naughton et al., 2009) were characterized by distinct NAO modes. The dynamics of the NAO and Azores High pressure system prior to the historical era are only beginning to be understood (Trouet et al., 2009; Olsen et al., 2012; Wassenburg et al., 2013), and the BG/GCL record cannot address this question independently. However, rainfall variability in eastern Iberia is less closely tied to the NAO than is western Iberia and instead reflects other climatic phenomena including the El Niño-Southern Oscillation (Rodó et al., 1997), helping to produce an east-west precipitation gradient. Additional high-resolution speleothem records from central and eastern Iberia could therefore provide a more robust test of the underlying drivers of millennial-scale hydroclimatic changes during recent glacial periods.

6. Conclusions

The BG/GCL composite speleothem record demonstrates that the hydroclimate and vegetation dynamics in west-central Portugal tracked Iberian margin SST over orbital and millennial scales during the past two glacial cycles. Enhanced aridity characterized HS, as evidenced by elevated carbon and oxygen isotopic ratios and/or hiatuses in stalagmite growth, consistent with other regional stalagmite time series. GI/GS variability expressed in the Iberian margin SST record and in co-deposited pollen spectra is also present in the BG/GCL time series, and is particularly well defined in MIS 5a and 5b. Understanding differences between the structures of the stalagmite and SST records during some time intervals will require development of speleothem records from central and southern Iberia.

785 **Acknowledgements**

786 This work was supported by the Center for Global and Regional Environmental Research
787 and Cornell College (to R.F.D.), and the U.S. National Science Foundation (grant BCS-1118155
788 to J.A.H., BCS-1118183 to M.M.B., and AGS-135539 to C.C.U.). Field sampling performed
789 under the auspices of IGESPAR (to J.A.H.) and Associação de Estudos Subterrâneos e Defesa do
790 Ambiente. Brandon Zinsious and Stephen Rasin contributed to fieldwork at BG, and Zachary
791 LaPointe assisted with radioisotopic analyses; Suzanne Ankerstjerne performed stable isotope
792 measurements. Use of the following data sets is gratefully acknowledged: Global Precipitation
793 Climatology Center data by the German Weather Service (DWD) accessed through
794 <http://gpcc.dwd.de>; NAO Index Data provided by the Climate Analysis Section, NCAR, Boulder,
795 USA, Hurrell (2003). Updated regularly. Accessed through
796 [https://climatedataguide.ucar.edu/climate-data/hurrell-north-atlantic-oscillation-nao-index-pc-](https://climatedataguide.ucar.edu/climate-data/hurrell-north-atlantic-oscillation-nao-index-pc-based)
797 [based](#). This manuscript benefitted **greatly** from discussions with Maria F. Sánchez Goñi, David
798 Hodell, and Chronis Tzedakis. We thank four anonymous reviewers, whose detailed and
799 thoughtful assessment of the original version of this manuscript substantially improved its scope
800 and clarity. Stable and U-series isotope data are available at the NOAA National Centers for
801 Environmental Information website.

802

803 **References**

804 de Abreu, L., Shackleton, N.J., Schönfeld, J., Hall, M., and Chapman, M.: Millennial-scale
805 oceanic climate variability off the Western Iberian margin during the last two glacial periods,
806 Marine Geol, 196, 1-20, 2003.
807 Asmerom, Y., Polyak, V., Burns, S.: Variable winter moisture in the southwestern United States
808 linked to rapid glacial climate shifts, Nat Geosci, 3, 114-117, 2010.
809 Baker, A., Ito, E., Smart, P., McEwan, R.: Elevated and variable values of ¹³C in speleothems in
810 a British cave system, Chem Geol, 136, 263-270, 1997.
811 Barker, S., Knorr, G., Edwards, R.L., Parrenin, F., Putnam, A.E., Skinner, L.C., Wolff, E.,
812 Ziegler, M.: 800,000 years of abrupt climate variability, Science, 334, 347-351, 2011.
813 Bar-Matthews, M., Ayalon, A., Gilmour, M., Matthews, A., Hawkesworth, C.J.: Sea-land
814 oxygen isotopic relationships from planktonic foraminifera and speleothems in the Eastern

Rhawn Denniston 11/13/2018 4:16 PM
Deleted:

816 Mediterranean region and their implication for paleo-rainfall during interglacials intervals,
817 *Geochim Cosmochim Acta*, 67, 3181–3199, 2003.

818 Barnston, A.G. and Livezey, R.E.: Classification, seasonality, and persistence of low-frequency
819 atmospheric circulation patterns, *Mon Weather Rev*, 115, 1083–1126, 1987.

820 Berger, A. and Loutre, M.F.: Insolation values for the climate of the last 10 million years.
821 *Quaternary Sci Rev* 10, 297-318, 1991.

822 Blanco Castro, E., Casado González, M.A., Costa Tenorio, M., Escribano Bombín, R., García
823 Antón, M., Génova Fuster, M., Gómez Manzaneque, F., Gómez Manzaneque, A., Moreno
824 Sáiz, J.C., Morla Juaristi, C., Regato Pajares, P., Sáiz Ollero, H.: Los bosques ibéricos.
825 Planeta, Barcelona, 1997.

826 Boch, R., Cheng, H., Spötl, C., Edwards, R.L., Wang, X., Hauselmann, Ph.: NALPS: a precisely
827 dated European climate record 120-60 ka, *Clim Past*, 7, 1049-1072, 2011.

828 Breitenbach, S.F.M., Rehfeld, K., Goswami, B., Baldini, J.U.L., Ridley, H.E., Kennett, D.J.,
829 Prufer, K.M., Aquino, V.V., Asmerom, Y., Polyak, V.J., Cheng, H., Kurths, J., Marwan, N.:
830 Constructing proxy records from age models (COPRA), *Clim Past*, 8, 1765-1779, 2012.

831 Breitenbach, S.F.M., Lechleitner, F.A., Meyer, H., Diengdo, G., Matthey, D., Marwan, N.: Cave
832 ventilation and rainfall signals in dripwater in a monsoonal setting – a monitoring study from
833 NE India, *Chem Geol*, 402, 111-124, 2015.

834 CDG: The Climate Data Guide: Hurrell North Atlantic Oscillation (NAO) Index (PC-based).
835 Retrieved from [https://climatedataguide.ucar.edu/climate-data/hurrell-north-atlantic-](https://climatedataguide.ucar.edu/climate-data/hurrell-north-atlantic-oscillation-nao-index-pc-based)
836 [oscillation-nao-index-pc-based](https://climatedataguide.ucar.edu/climate-data/hurrell-north-atlantic-oscillation-nao-index-pc-based), accessed 21 May, 2018.

837 Chabaud, L., Sánchez Goñi, M.F., Desprat, S., Rossignol, L.: Land-sea climatic variability in the
838 eastern North Atlantic subtropical region over the last 14,200 years: Atmospheric and
839 oceanic processes at different timescales Holocene, 24, 787-797, 2014.

840 Chabaux, F., Riotte, J., Dequincey, O.: U–Th–Ra fractionations during weathering and river
841 transport. *Rev Mineral Geochem*, 52, 533–576. 2003.

842 Collister, C. and Matthey, D.: Controls on water drop volume at speleothem drip sites: An
843 experimental study. *J Hydrol*, 358, 259-267, 2008.

844 Combourieu-Nebout, N., Peyron, O., Dormoy, I., Desprat, S., Beaudouin, C., Kotthoff, U.,
845 Marret, F.: Rapid climatic variability in the west Mediterranean during the last 25 000 years
846 from high resolution pollen data, *Clim Past*, 5, 503-521, 2009.

847 Cortesi, N., Gonzalez-Hidalgo, J.C., Trigo, R.M., and Ramos, A.M.: Weather types and spatial
848 variability of precipitation in the Iberian Peninsula. *International Journal of Climatology*, 34,
849 2661-2677, 2014.

850 Couchoud, I, Genty, D., Hoffman, D., Drysdale, R., Blamart, D.: Millennial-scale climate
851 variability during the Last Interglacial recorded in a speleothem from south-western France.
852 *Quaternary Sci Rev*, 28, 3263-3274, 2009.

853 Daniau, A.-L., Sánchez Goñi, M.F., Beaufort, L., Laggoun-Defarge, F., Loutre, M.-F., Duprat, J.:
854 Dansgaard-Oeschger climatic variability revealed by fire emissions in southwestern Iberia.
855 *Quaternary Sci Rev*, 26, 1369-1383, 2007.

856 Darfeuil, S., Ménot, G., Giraud, X., Rostek, F., Tachikawa, K., Garcia, M., Bard, É.: Sea surface
857 temperature reconstructions over the last 70 kyr off Portugal: Biomarker data and regional
858 modeling, *Paleocean*, 31, 40–65, 2016.

859 Deines, P.: The isotopic composition of reduced organic carbon. *Handbook of Environmental*
860 *Isotope Geochemistry, The Terrestrial Environment, Part A* (Fritz, P. and Fontes, J., Eds.,
861 Elsevier, New York, 331-406, 1980.

862 Denniston, R.F., González, L.A., Asmerom, Y., Baker, R.G., Reagan, M.K. Bettis, E.A. III.:
863 Evidence for increased cool season moisture during the middle Holocene, *Geology*, 27, 815-
864 818, 1999.

865 Denniston, R.F., Wyrwoll, K.-H., Polyak, Brown, J. Asmerom, Y., Wanamaker, A. Jr., LaPointe
866 Z., Ellerbroek, R., Barthelmes, M., Cleary, D., Cugley, J., Woods, D., Humphreys, W.: A
867 Stalagmite Record of Holocene Indonesian-Australian Summer Monsoon Variability from
868 the Australian Tropics. *Quaternary Sci Rev* 78, 155-168, 2013.

869 Desprat et al.: Climatic variability of Marine Isotope Stage 7: direct land-sea-ice correlation from
870 a multiproxy analysis of a north-western Iberian margin deep-sea core. *Quaternary Sci Rev*
871 25, 1010-1026, 2006.

872 Desprat, S., Sánchez Goñi, M.F., Naughton, F., Turon, J.-L., Duprat, J., Malaizé, B., Cortijo, E.,
873 Peyrouquet, J.-P.: Climate variability of the last five isotopic interglacials: Direct land-sea-
874 ice correlation from the multiproxy analysis of North-Western Iberian margin deep-sea cores,
875 Editor(s): F. Sirocko, M. Claussen, M.F. Sánchez Goñi, T. Litt *In* *Developments in*
876 *Quaternary Sciences*, Elsevier, pp. 375-386, 2007.

877 Dorale, J.A., and Liu, Z.: Limitations of Hendy Test criteria in judging the paleoclimatic
878 suitability of speleothems and the need for replication. *J Cave Karst Stud*, 71, 73-80, 2009.

879 Dreybott, W.: Evolution of the isotopic composition of carbon and oxygen in a calcite
880 precipitating H₂O-CO₂-CaCO₃ solution and the related isotopic composition of calcite in
881 stalagmites. *Geochim. Cosmochim. Acta*, 72, 4712-4724, 2008.

882 Eynaud et al.: Position of the Polar Front along the western Iberian margin during key cold
883 episodes of the last 45 ka, *Geochim Geophys Geosys*, 10, Q07U05,
884 doi:10.1029/2009GC002398, 2009.

885 Fairchild, I.J., Smith, C.L., Baker, A., Fuller, L., Spötl, C., Mathey, D., McDermott, F., E.I.M.F.:
886 Modification and preservation of environmental signals in speleothems. *Earth Sci Rev* 75,
887 105-153, 2006.

888 Fankhauser, A., McDermott, F., and Fleitmann, D.: Episodic speleothem deposition tracks the
889 terrestrial impact of millennial-scale last glacial climate variability in SW Ireland, *Quaternary*
890 *Sci Rev*, 152, 104-117, 2016.

891 von Fischer, J.C., Tieszen, L.L., and Schimel, D.S.: Climate controls on C₃ vs. C₄ productivity in
892 North American grasslands from carbon isotope composition of soil organic matter. *Global*
893 *Change Bio*, 14, 1-15, 2008.

894 Fletcher, W.J., Sánchez Goñi, M.F., Allen, J.R.M., Cheddadi, R., Combouieu-Nebout, N.,
895 Huntley, B., Lawson, I., Londeix, L., Magri, D., Margari, v., Müller, U.C., Naughton, F.,
896 Novenko, E., Roucoux, K., Tzedakis, P.C.: Millennial scale variability during the last glacial
897 in vegetation records from Europe. *Quaternary Sci Rev*, 29, 2839-2864, 2010.

898 Florineth, D. and Schlüchter, S. Alpine Evidence for Atmospheric Circulation Patterns in Europe
899 during the Last Glacial Maximum. *Quaternary Research*, 54, 295-308, 2000.

900 Francey, R. J., Allison, C. E., Etheridge, D. M., Trudinger, C. M., Enting, I. G., Leuenberger, M.,
901 Langenfelds, R. L., Michel, E., and Steele, L. P. A.: 1000-year high precision record of ¹³C in
902 atmospheric CO₂. *Tellus B: Chemical and Physical Meteorology*, 51, 170-193, 1999.

903 Genty, D., Blamart, D., Ouahdi, R., Gilmour, M., Baker, A., Jouzel, J., Van-Exter, S.: Precise
904 dating of Dansgaard-Oeschger climate oscillations in western Europe from stalagmite data,
905 *Nature*, 421, 833-837, 2003.

906 Genty, D., Combouieu-Nebout, N., Peyron, O., Blamart, D., Wainer, K., Mansuri, F., Ghaleb,
907 B., Isabello, L., Dormoy, I., von Grafenstein, U., Bonelli, S., Landais, A., Brauer, A.:

908 Isotopic characterization of rapid climatic events during OIS3 and OIS4 in Villars Cave
 909 stalagmites (SW-France) and correlation with Atlantic and Mediterranean pollen records.
 910 Quaternary Sci. Rev., 29, 2799-2820, 2010.

911 Genty, D., Blamart, D., Ghaleb, B., Plagnes, V., Causse, Ch., Bakalowicz, M., Zouari, K., Chkir,
 912 N., Hellstrom, J., Wainer, K., and Bourges, F.: Timing and dynamics of the last deglaciation
 913 from European and North African $\delta^{13}\text{C}$ stalagmite profiles – comparison with Chinese and
 914 South Hemisphere stalagmites. Quaternary Sci Rev 25, 2118-2142, 2006.

915 Gimeno, L., Nieto, R., Trigo, R.M., Vicente-Serrano, S.M., and López-Moreno, J.I., Where does
 916 the Iberian Peninsula moisture come from? An answer based on a Lagrangian approach. J.
 917 Hydrometeorology, 11, 421-436, 2010.

918 Gimeno, L., Stohl, A., Trigo, R.M., Dominguez, F., Yoshimura, K., Yu., L., Drumond, A.,
 919 Durán-Quesada, A.M., Nieto, R.: Oceanic and terrestrial sources of continental precipitation.
 920 Rev Geophy, 50, 1-41, 2012.

921 Gómez-Orellana, L., Ramil-Rego, P., & Sobrino, C. M.: The Würm in NW Iberia, a pollen
 922 record from Area Longa (Galicia). Quaternary Res, 67, 438-452, 2008.

923 Grootes, P. M.: *Climate Change in Continental Isotopic Records*, P. K. Swart, K. C. Lohmann, J.
 924 McKenzie, S. Savin, Eds. (American Geophysical Union, Washington, DC), pp. 37- 46,
 925 1993.

926 Hellstrom, J. and McCulloch, M.: Multi-proxy constraints on the climatic significance of trace
 927 element records from a New Zealand speleothem. Earth Planet Sci Lett, 179, 287-297, 2000.

928 Hendy, C.: The isotopic geochemistry of speleothems – I. The calculation of the effects of
 929 different modes of formation on the isotopic composition of speleothems and their
 930 applicability as palaeoclimatic indicators. Geochimica et Cosmochimica Acta 35, 801-824,
 931 1971.

932 Herbert, T.D., Schuffert, J.D., Heusser, L., Lyle, M., Mix, A., Ravelo, A.C., Stott, L.D., and
 933 Herguera, J.C.: Collapse of the California current during glacial maxima linked to climate
 934 change on land. Science, 293, 71-76, 2001.

935 Hodell, D., Crowhurst, S., Skinner, L., Tzedakis, P.C., Margari, V., Channell, J.E.T., Kamenov,
 936 G., Maclachlan, S., Rothwell, G.: Response of Iberian margin sediments to orbital and
 937 suborbital forcing over the past 420 ka, Paleoceanography, 28, 185-199, 2013.

938 Hodge, E.J., Richards, D.A., Smart, P.L., Andreo, B., Hoffman, D.L., Matthey, D.P., Gonzales-
 939 Ramon, A.: Effective precipitation in southern Spain (~266 to 46 ka) based on a speleothem
 940 stable carbon isotope record. *Quaternary Res*, 69, 447-457, 2008.
 941 IAEA/WMO: Global Network of Isotopes in Precipitation. The GNIP Database. Accessible at:
 942 <http://www.iaea.org/water>, 2016.
 943 IPMA: Accessible at <http://www.meteo.pt/en/oclima/clima.normais/015/>, 2012.
 944 Justino, F. and Peltier, W.R.: The glacial North Atlantic Oscillation. *Geophysical Research*
 945 *Letters*, 32, L21803, 2008.
 946 Kim, S.-T. and O'Neil, J.R.: Equilibrium and nonequilibrium oxygen isotope effects in synthetic
 947 carbonates: *Geochim Cosmochim Acta*, 61, 3461-3475, 1997.
 948 Kuhlemann, J et al.: Regional synthesis of Mediterranean atmospheric circulation during the Last
 949 Glacial Maximum. *Science*, 321, 1338– 1340, 2008.
 950 Lachniet, M.S.: Climatic and environmental controls on speleothem oxygen isotope values.
 951 *Quaternary Sci Rev* 28, 412-432, 2009.
 952 Lechleitner, F.A., Breitenbach, S.F.M., Cheng, H., Plessen, B.: Climatic and in-cave influences
 953 on $\delta^{18}\text{O}$ and $\delta^{13}\text{C}$ in a stalagmite from northeastern India through the last deglaciation. *Quat*
 954 *Res*, 88, 458-471, 2017.
 955 Li, Z.-H., Driese, S.G., Cheng, H.: A multiple cave deposit assessment of suitability of
 956 speleothem isotopes for reconstructing palaeo-vegetation and palaeo-temperature.
 957 *Sedimentology*, 61, 749-766, 2014.
 958 Lorenzo, M.N., Iglesias, I., Taboada, J.J., Gomez-Gesteira, M.: Relationship between monthly
 959 rainfall in northwest Iberian Peninsula and North Atlantic sea surface temperature. *Int J*
 960 *Climatology*, 30, 980-990, 2010.
 961 Loulergue, L., Schilt, A., Spahni, R., Masson-Delmotte, V., Blunier, T., Lemieux, B., Barnola,
 962 J.-M., Raynaud, D., Stocker, T.F., Chappellaz, J.: Orbital and millennial-scale features of
 963 atmospheric CH_4 over the past 800,000 years, *Nature*, 453, 383-386, 2008.
 964 Luetscher, M., Boch, R., Sodemann, H., Spötl, C., Cheng, H., Edwards, R.L., Frisia, S., Hof, F.,
 965 and Müller, W.: North Atlantic storm track changes during the Last Glacial Maximum
 966 recorded by Alpine speleothems. *Nature Communications*, 6, DOI: 10.1038/ncomms7344,
 967 2016.

968 Margari, V., Skinner, L.C., Tzedakis, P.C., Ganopolski, A., Vautravers, M., and Shackleton,
 969 N.J.: The nature of millennial-scale climate variability during the past two glacial periods:
 970 Nature Geoscience, v. 3, p. 127–131, doi:10.1038/ngeo740, 2010.
 971 Margari, V., Skinner, L.C., Hodell, D.A., Martrat, B., Toucanne, S., Grimalt, J.O., Gibbard, P.L.,
 972 Lunkka, J.P., Tzedakis, P.C.: Land-ocean changes on orbital and millennial time scales and
 973 the penultimate glaciation, *Geology*, 42, 183-186, 2014.
 974 Martin-Vide, J. and Lopez-Bustins, J-A.: The Western Mediterranean Oscillation and rainfall in
 975 the Iberian Peninsula. *Int J Climatol*, 26, 1455-1475, 2006.
 976 Martrat, B., Grimalt, J.O., Shackleton, N.J., de Abreu, L., Hutterli, M.A., Stocker, T.F.: Four
 977 climate cycles of recurring deep and surface water destabilizations on the Iberian margin,
 978 *Science*, 317, 502-507, 2007.
 979 McManus, J.F., Oppo, D.W., Cullen, J.L.: A 0.5-Million-Year Record of Millennial-Scale
 980 Climate Variability in the North Atlantic, *Science*, 283, 971-975, 1999.
 981 Mickler, P.J. et al.: Stable isotope variations in modern tropical speleothems: Evaluation
 982 equilibrium vs. kinetic isotope effects. *Geochim Cosmochim Acta*. 68, 4381-4393, 2004.
 983 Moreno, A., Cacho, I., Canals, M., Prins, M.A., Sánchez Goñi, M.F., Grimalt, J.O., Weltje, G.J.:
 984 Saharan dust transport and high-latitude glacial climate variability: the Alboran Sea record.
 985 *Quaternary Res*, 58, 318-328, 2002.
 986 Moreno, A., Gonzalez-Samperiz, P., Morellon, M., Valero-Garces, B.L., Fletcher, W.J.:
 987 Northern Iberian abrupt climate change dynamics during the last glacial cycle: a view from
 988 lacustrine sediments. *Quaternary Sci Rev*, 36, 139-153, 2012.
 989 Moreno, A., Sancho, C., Bartolomé, M., Oliva-Rucia, B., Delgado-Huertas, A., José, Estrela, M.,
 990 Corell, D., López-Moreno, J.I., Cacho, I.: Climate controls on rainfall isotopes and their
 991 effects on cave drip water and speleothem growth: the case of Molinos cave (Teruel, NE
 992 Spain). *Clim Dyn*, 43, 221-241, 2014.
 993 Moseley, G.E., Spötl, C., Scensson, A., Cheng, H., Brandstatter, S., Edwards, R.L.: Multi-
 994 speleothem record reveals tightly coupled climate between central Europe and Greenland
 995 during Marine Isotope Stage 3. *Geology*, 42, 1043-1046, 2014.
 996 Mühlinghaus, C., Scholz, D., and Mangini, A.: Modelling stalagmite growth and $\delta^{13}C$ as a
 997 function of drip interval and temperature. *Geochim. Cosmochim. Acta*, 71, 2780-2790, 2007.

998 Naughton, F., Sánchez Goñi, M.F., Desprat, S., Turon, J.-L., Duprat, J., Malaizé, B., Joli, C.,
 999 Cortijo, E., Drago, T., Freitas, M.C.: Present-day and past (last 25,000 years) marine pollen
 1000 signal off western Iberia. *Mar Micropaleontol*, 62, 91–114, 2007.
 1001 Naughton, F., Sánchez Goñi, M.F., Kageyama, M., Bard, E., Duprat, J., Cortijo, E., Desprat, S.,
 1002 Malaizé, B., Joly, C., Rostek, F., Turon, J.-L.: Wet to dry climatic trend in north-western
 1003 Iberia within Heinrich events. *Earth Planet Sc Lett*, 284, 329–342, 2009.
 1004 North Greenland Ice Core Project members: High-resolution record of Northern Hemisphere
 1005 climate extending into the last interglacial period, *Nature*, 431, 147–151, 2004.
 1006 Olsen, J., Anderson, N.J., and Knudsen, M.F.: Variability of the North Atlantic Oscillation over
 1007 the past 5,200 years. *Nature Geoscience*, 5, 808–812, 2012.
 1008 Oster, J.L., Ibarra, D.L., Harris, C.H., Maher, K.: Influence of eolian deposition and rainfall
 1009 amounts on the U-isotopic composition of soil water and soil minerals. *Geochim Cosmochim*
 1010 *Ac*, 88, 146 – 166, 2012.
 1011 Paredes, D., Trigo, R.M., Garcia-Herrera, R., Franco Trigo, I.: Understanding precipitation
 1012 changes in Iberia in early spring: weather typing and storm-tracking approaches. *J*
 1013 *Hydrometeorol*, 7, 101–113, 2006.
 1014 Petit, J.R., Jouzel, J., Raynaud, D., Barkov, N.I., Barnola, J.-M., Basile, I., Bender, M.,
 1015 Chappellaz, J., Davis, M., Delaygue, G., Delmotte, M., Kotlyakov, V.M., Legrand, M.,
 1016 Lipenkov, V.Y., Lorius, C., Pepin, L., Ritz, C., Saltzman, E., Stievenard, M.: Climate and
 1017 atmospheric history of the 420,000 years from the Vostok ice core, Antarctica. *Nature*, 399,
 1018 429–436, 1999.
 1019 Plagnes, V., Causse, C., Genty, D., Paterne, M., Blamart, D.: A discontinuous climatic record
 1020 from 187 to 74 ka from a speleothem of the Clamouse Cave (south of France). *Earth Planet*
 1021 *Sci Lett*, 201, 87–103, 2002.
 1022 Polyak, V.J., Asmerom, Y., Burns, S.J., and Lachniet, M.S.: Climatic backdrop to the terminal
 1023 Pleistocene extinction of North American mammals, *Geology*, 40, 1023–1026, 2012.
 1024 Rasmussen, S.O. et al.: A stratigraphic framework for abrupt climatic changes during the Last
 1025 Glacial period based on three synchronized Greenland ice-core records: redefining and
 1026 extending the INTIMATE event stratigraphy, *Quaternary Sci Rev*, 106, 14–28, 2014.
 1027 Rey Benayas, J.M. and Scheiner, S.M.: Plant diversity, biogeography and environment in Iberia:
 1028 Patterns and possible causal factors. *J Veg Sci*, 13, 245–258, 2002.

1029 Rodó, X., Baert, E., Comin, F.A.: Variations in seasonal rainfall in Southern Europe during the
 1030 present century: relationships with the North Atlantic Oscillation and the El Niño-Southern
 1031 Oscillation. *Clim Dynam*, 13, 275-284, 1997.
 1032 Rodrigues et al.: The last glacial-interglacial transition (LGIT) in the western mid-latitudes of the
 1033 North Atlantic: Abrupt sea surface temperature change and sea level implications.
 1034 *Quaternary Sci Rev*, 29, 1853-1862, 2010.
 1035 Roucoux, K.H., de Abreu, L., Shackleton, N.J., Tzedakis, P.C.: The response of NW Iberian
 1036 vegetation to North Atlantic climate oscillations during the last 65kyr, *Quaternary Sci Rev*,
 1037 24, 1637-1653, 2005.
 1038 Roucoux, K.H., Tzedakis, P.C., de Abreu, L., Shackleton, N.J.: Climate and vegetation changes
 1039 180,000 to 345,000 years ago recorded in a deep-sea core off Portugal. *Earth Planet Sci Lett*,
 1040 249, 307-325, 2006.
 1041 Rousseau, D.D., Kukla, G., McManus, J.: What is what in the ice and the ocean? *Quaternary Sci*
 1042 *Rev*, 25, 2025-2030, 2006.
 1043 K. L. Rosanski, Araguas-Araguas, R. Gonfiantini, in *Climate Change in Continental Isotopic*
 1044 *Records*, P. K. Swart, K. C. Lohmann, J. McKenzie, S. Savin, Eds. (American Geophysical
 1045 Union, Washington, DC), pp. 1–36, 1993.
 1046 Saltzman, Matthew & Thomas, E. (2012). Carbon Isotope Stratigraphy. *The Geologic Time*
 1047 *Scale*, 1, 207-232. 2012.
 1048 Sánchez Goñi, M.F., Turon, J.L., Eynaud, F., Gendreau, S., European climatic response to
 1049 millennial-scale changes in the atmosphere-ocean system during the Last Glacial Period.
 1050 *Quaternary Res*, 54, 394-403, 2000.
 1051 Sánchez Goñi, M.F., Cacho, I., Turon, J-L., Guiot, J., Sierro, F.J., Peyrouquet, J.-P., Grimalt,
 1052 J.O., Shackleton, N.J.: Synchronicity between marine and terrestrial responses to millennial
 1053 scale climatic variability during the last glacial period in the Mediterranean region. *Clim*
 1054 *Dynam*, 19, 95-105, 2002.
 1055 Sánchez Goñi, M.F., Landais, A., Fletcher, W.J., Naughton, F., Desprat, S., Duprat, J.:
 1056 Contrasting impacts of Dansgaard-Oeschger events over a western European latitudinal
 1057 transect modulated by orbital precession. *Quaternary Sci Rev*, 27, 1136-1151, 2008.

1058 Sánchez Goñi, M.F., Bard, E., Landais, A., Rossignol, L., d'Errico, F.: Air-sea temperature
 1059 decoupling in western Europe during the last interglacial-glacial transition. *Nat Geosci*, 6,
 1060 837-841, 2013.

1061 Sánchez Goñi, M.F., Rodrigues, T., Hodell, D.A., Polanco-Martinez, J.M., Alonso-Garcia, M.,
 1062 Hernandez-Almeida, I., Desprat, S., Ferretti, P.: Tropically-driven climate shifts in
 1063 southwestern Europe during MIS 19, a low eccentricity interglacial. *Geophys Res Abst*, 18,
 1064 EGU2016-3940, 2016.

1065 Schneider, U., Becker, A., Finger, P., Meyer-Christoffer, A., Ziese, M., Rudolf, B.: GPCC's new
 1066 land surface precipitation climatology based on quality-controlled in situ data and its role in
 1067 quantifying the global water cycle. *Theoret Appl Climatol*, 115, 15-40, 2013.

1068 Schneider, U., A. Becker, P. Finger, A. Meyer-Christoffer, M. Ziese, and B. Rudolf (2014),
 1069 GPCC's new land surface precipitation climatology based on quality-controlled in situ data
 1070 and its role in quantifying the global water cycle, *Theor. Appl. Climatol.*, 115, 1–15.

1071 Schrag, D.P, Hampt, G., and Murray, D.W.: Pore fluid constraints on the temperature and
 1072 oxygen isotopic composition of the glacial ocean. *Science*, 272, 5270, 1930-1932, 1996.

1073 Spötl, C., Mangini, A., Richards, D.A.: Chronology and paleoenvironment of Marine Isotope
 1074 Stage 3 from two high-elevation speleothems, Austrian Alps. *Quaternary Sci Rev*, 25, 1127-
 1075 1136, 2006.

1076 Stoll, H.M., Moreno, A., Mendez-Vincente, A., Gonzalez-Lemos, S., Jimenez-Sánchez, M.,
 1077 Dominguez-Cuesta, M.J., Edwards, R.L., Cheng, H., Wang, X.: Paleoclimate and growth
 1078 rates of speleothems in the northwestern Iberian Peninsula over the last two glacial cycles.
 1079 *Quaternary Res*, 80, 284-290, 2013.

1080 Thatcher, D.L., Wanamaker, A.D., Jr., Denniston, R.F., Asmerom, Y., Ummenhofer, C.C.,
 1081 Polyak, V.J., Hasiuk, F., Haws, J.A., and Gillikin, D.P.: Changes in hydroclimate in Iberia in
 1082 the last 1200 years: insights from speleothem records from western Portugal. *Geological*
 1083 *Society of America North-Central Meeting Abstracts with Programs*, Ames, Iowa, 2018.

1084 Trigo, R.M., Osborn, T.J., Corte-Real, J.M.: The North Atlantic Oscillation influence on Europe:
 1085 climate impacts and associated physical mechanisms, *Clim Res*, 20, 9-17, 2002.

1086 Trouet, V., Esper, J., Graham, N.E., Baker, A., Scourse, J.D., Grank, D.C.: Persistent positive
 1087 North Atlantic Oscillation mode dominated the Medieval Climate Anomaly. *Science*, 324,
 1088 78-80, 2009.

1089 Tzedakis, P.C., Roucoux, K.H., de Abreu, L., Shackleton, N.J.: The duration of forest stages in
1090 southern Europe and interglacial climate variability, *Science*, 306, 2231-2235, 2004.

1091 Vaks, A., Gutareva, O.S., Breitenbach, S.F.M., Avirmed, E., Mason, A.J., Thomas, A.L., Osinev,
1092 A.V., Kononov, A.M., Henderson, G.M.: Speleothems reveal 500,000-year history of
1093 Siberian permafrost. *Science*, 340, 183-186, 2013.

1094 Vandenberghe, J., French, H.M., Gorbunov, A., Marchenko, S., Velichko, A.A., Jin, H., Cui,
1095 Z., Zhang, T., Wan, X.: The Last Permafrost Maximum (LPM) map of the Northern
1096 Hemisphere: permafrost extent and mean annual air temperatures, 25-17 ka BP, *Boreas*, 43,
1097 652–666, 2014.

1098 Vegas, J., Ruiz-Zapata, B., Ortiz, J.E., Galan, L., Torres, T., Garcia-Cortes, A., Gil-Garcia, M.J.,
1099 Perez-Gonzalez, A., Gallardo-Millan, J.L.: Identification of arid phases during the last 50 cal.
1100 ka BP from the Fuentillejo maar-lacustrine record (Campo de Calatrava Volcanic Field,
1101 Spain), *J Quaternary Sci*, 25, 1051-1062, 2010.

1102 Voelker, A.H. L., Rodrigues, T., Stein, R., Hefter, J., Billups, K., Oppo, D., McManus, J.,
1103 Grimalt, J.O.: Variations in mid-latitude North Atlantic surface water properties during the
1104 mid-Brunhes (MIS 9-14) and their implications for thermohaline circulation, *Clim Past*, 6, p.
1105 531-552, 2010.

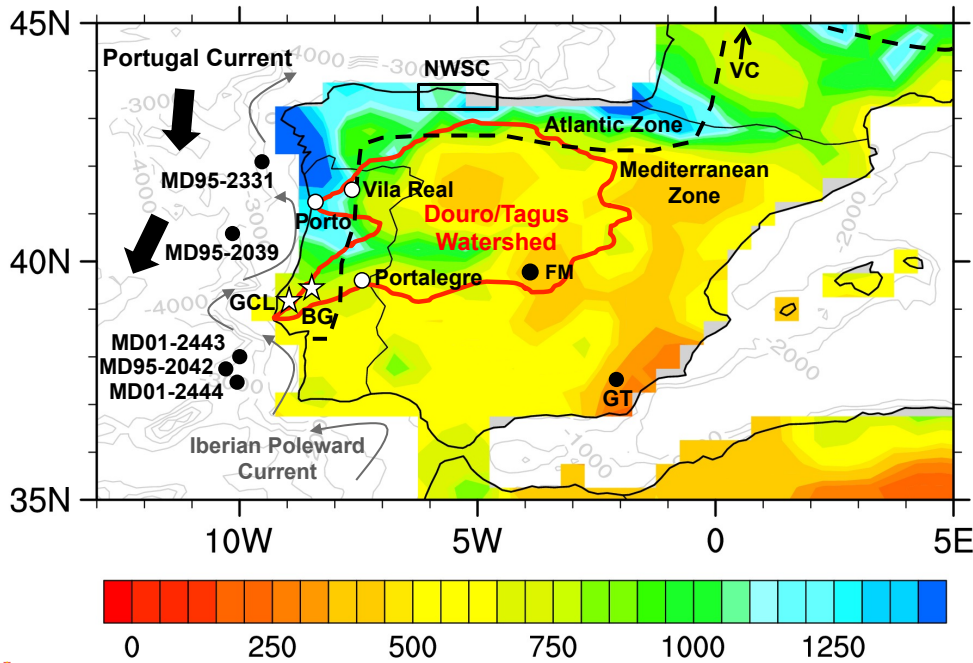
1106 Voelker, A.H.L. and de Abreu, L.: A review of abrupt climate change events in the northeastern
1107 Atlantic Ocean (Iberian Margin): Latitudinal, Longitudinal, and Vertical Gradients. *Abrupt*
1108 *Climate Change: Mechanisms, Patterns, and Impacts* (Eds. Rashid, H., Polyak, L., and
1109 Mosley-Thompson, E.), *Geophysical Monograph Series* 193, 15-37, 2011.

1110 Wainer, K., Genty, D., Blamart, D., Daëron, M., Bar-Matthews, M., Vonhof, H., Dublyansky,
1111 Y., Pons-Branchu, E., Thomas, L., van Calsteren, P., Quinif, Y., and Caillon, N.: Speleothem
1112 record of the last 180 ka in Villars cave (SW France): Investigation of a large $\delta^{18}\text{O}$ shift
1113 between MIS6 and MIS5. *Quaternary Sci. Rev.*, 30, 130-146, 2011.

1114 Wassenburg, J.A., Immenhauser, A., Richter, D.K., Niedermayr, A., Riechelmann, S., Fietzke,
1115 J., Scholz, D., Jochum, K.P., Fohlmeister, J., Schröder-Ritzrau, Sabaoui, A., Riechelmann,
1116 D.F.C., Schneider, L., Esper, J.: Moroccan speleothem and tree ring records suggest a
1117 variable positive state of the North Atlantic Oscillation during the Medieval Warm Period.
1118 *Earth Planet. Sci. Lett.*, 375, 291-302, 2013.

1119 Zhou, J., Lundstrom, C.C., Fouke, B., Panno, S., Hackley, K., and Curry, B. Geochemistry of
1120 speleothem records from southern Illinois: Development of (^{234}U)/(^{238}U) as a proxy for
1121 paleoprecipitation. Chemical Geology, 221, 1-20, 2005.
1122

1123



1124

1125

1126

1127 **Figure 1. Average annual precipitation (mm) of the Iberian Peninsula for years AD 1901-**
1128 **2009 (GPCC v. 6; Schneider et al., 2013) relative to cave study sites (white stars: GLC =**
1129 **Gruta do Casal da Lebre; BG = Buraca Gloriosa). Rectangle denotes location of northwest**
1130 **Spain cave sites (NWSC) (Moreno et al., 2010; Stoll et al., 2013); FM = Fuentillejo maar (Vegas**
1131 **et al., 2010) and GT = Gitana cave (Hodge et al., 2008); VC = Villars Cave (Genty et al., 2003)**
1132 **located just north of map. Also shown are locations of marine cores discussed in text and GNIP**
1133 **stations at Porto, Vila Real, and Portalegre. Bathymetric contours shown in grey (m). Location of**
1134 **currents after Voelker et al. (2010).**

1135

1136

Rhawn Denniston 11/13/2018 4:16 PM

Deleted:

Unknown

Formatted: Font:(Default) Times New Roman

Unknown

Formatted: Font:(Default) Times New Roman

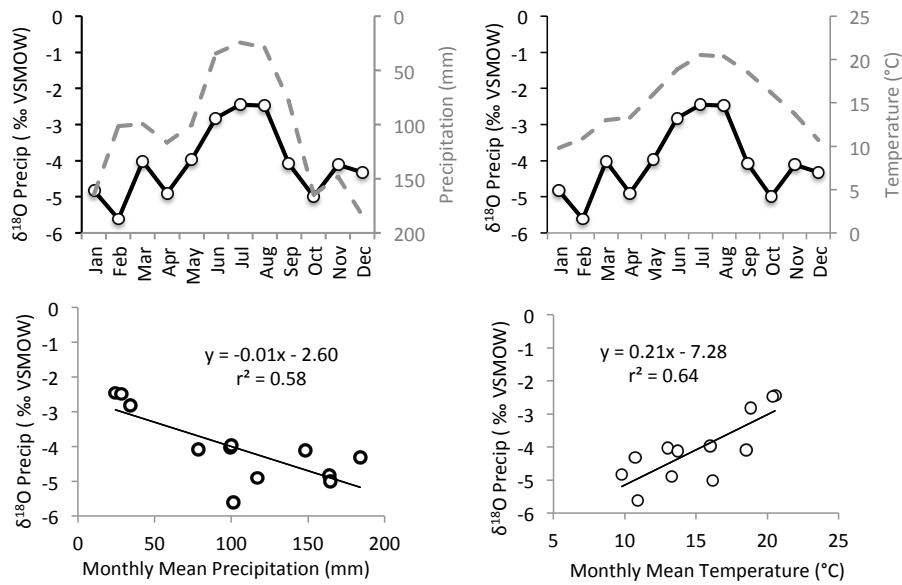


Figure 2. Oxygen isotopic composition of precipitation versus rainfall amount (lefthand panels) and air temperature (righthand panels). Data collected at IAEA/GNIP site in Porto, Portugal (see Fig. 1 for location) for 1988-2004. Oxygen isotope data represent multi-year averages of monthly means. The two other closest GNIP stations in Portugal - Vila Real and Portalegre (see Figure 1) - share similar relationships between precipitation oxygen isotopic composition and air temperature ($+0.27\text{‰}/^{\circ}\text{C}$: $r^2=0.76$ and $+0.26\text{‰}/^{\circ}\text{C}$; $r^2=0.69$, respectively) to that of Porto ($+0.21\text{‰}/^{\circ}\text{C}$). The relationship between precipitation oxygen isotopic composition and monthly precipitation amount is $-3.5\text{‰}/100\text{mm}/\text{month}$ ($r^2=0.64$), $-3.7\text{‰}/100\text{mm}/\text{month}$ ($r^2=0.49$), and $-1.6\text{‰}/100\text{mm}/\text{month}$ ($r^2=0.62$) for the three sites, respectively. Note that right hand y-axis in upper left panel is inverted in order to illustrate inverse nature of rainfall and precipitation oxygen isotopic composition.

Rhawn Denniston 11/13/2018 4:16 PM

Deleted:

Unknown

Formatted: Font:(Default) Times New Roman

Unknown

Formatted: Font:(Default) Times New Roman

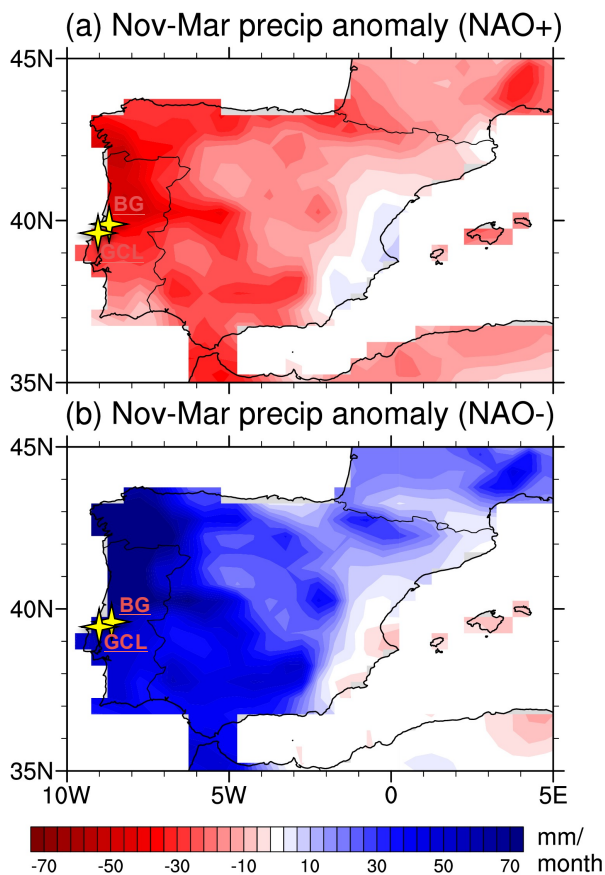


Figure 3. Iberian rainfall anomalies associated with the North Atlantic Oscillation. Composites of November-March precipitation anomalies (mm/month) during (a) positive and (b) negative NAO winters for the period 1901-2012. Positive/negative NAO winters were determined using the December-March Hurrell principal component-based NAO index (CDG, 2018) as those winters with NAO values in the highest/lowest decile of all winters. The PC-based NAO index represents the time series of the leading Empirical Orthogonal Function of SLP anomalies over the Atlantic sector, 20°-80°N, 90°W-40°E. Precipitation anomalies are based on the GPCC precipitation, version 7, at 0.5° spatial resolution (Schneider et al. 2014). Yellow stars denote cave sites in this study: BG = Buraca Gloriosa; GCL = Gruta do Casal da Lebre.

Rhawn Denniston 11/13/2018 4:16 PM

Deleted:

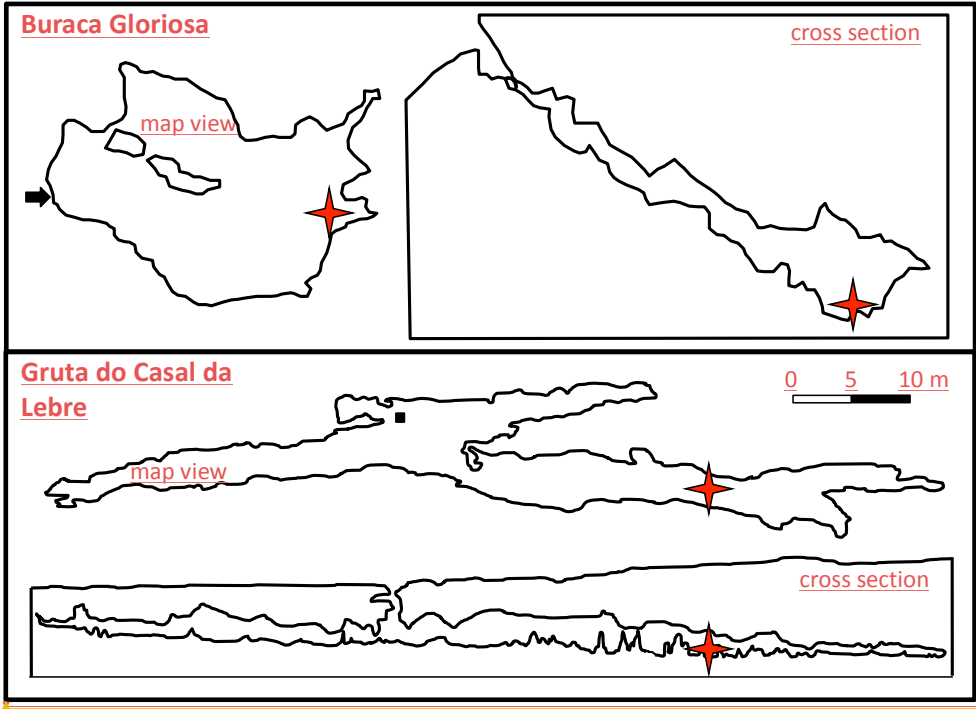
Unknown

Formatted: Font:(Default) Times New Roman

Unknown

Formatted: Font:(Default) Times New Roman

1167



1168

1169

1170 **Figure 4.** Profile and map views of Buraca Gloriosa (top) and Gruta do Casal da Lebre (bottom).

1171 Entrance denoted by arrow (top panel) and filled square (bottom panel). Red stars denote

1172 locations of stalagmites used in this study.

1173

Rhawn Denniston 11/13/2018 4:16 PM

Deleted:

Unknown

Formatted: Font:(Default) Times New Roman

Unknown

Formatted: Font:(Default) Times New Roman

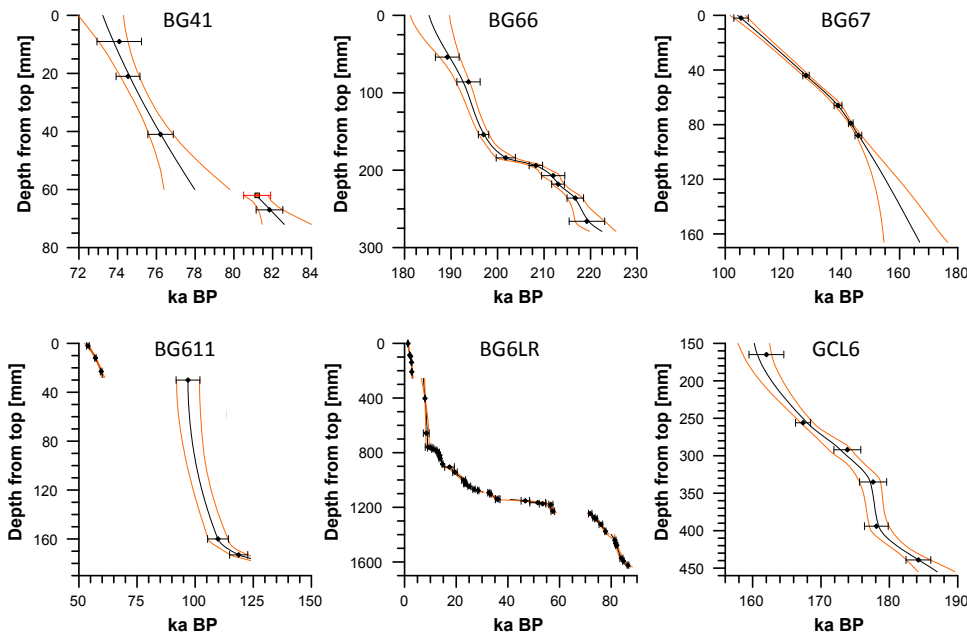


Figure 5. COPRA-derived age models for BG/GCL stalagmites. Black lines represent mean of calculated age models while red lines denote 95% confidence intervals. See Table 1 for specific ages and isotopic ratios. Orange square represents a “dummy age” that was included in order to extrapolate below the hiatus, which is only possible with at least two dated points. The bottom of BG611 was based on linear extrapolation through dated intervals. Distances for BG66 were measured relative to topmost section of interval for which stable isotopes were obtained, and not relative to the cap of the stalagmite (see Figure 6).

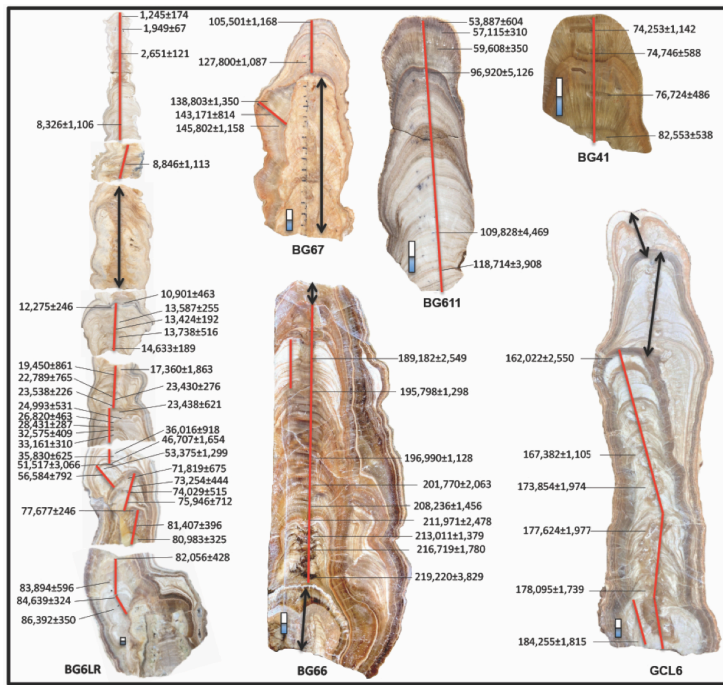


Figure 6. BG/GCL stalagmites and U/Th ages. Red lines denote stable isotope sampling transects. Blue and white scale bars (cm) define differential enlargement of each stalagmite. Black arrows represent intervals excluded from this study due to evidence of open system behavior. Sections without arrows or transect lines are older than the interval examined in this study. The impact of recrystallization in stalagmite cores was assessed by parallel sampling transects (parallel red lines on BG66 and GCL6) and demonstrated consistent stable isotopic values and trends (Supp. Fig. S7).

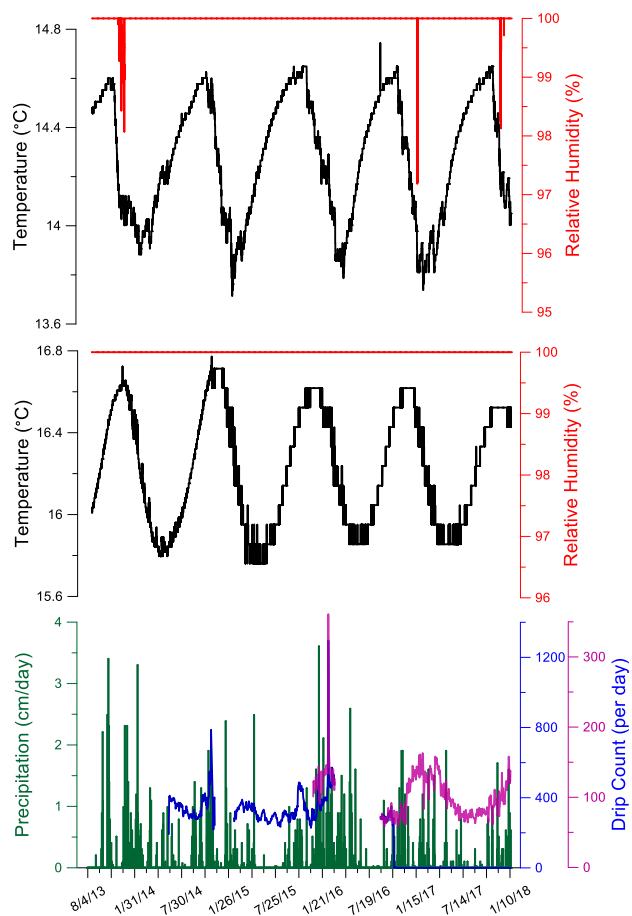


Figure 7. Temperature and relative humidity variations from (top) Buraca Gloriosa and (middle) GCL. Drip rate from Buraca Gloriosa and precipitation variability (bottom) from Monte Real, Portugal (35 km from BG). Temperature sensor in GCL was changed in November 2014 and the sensitivity of the new instrument varies slightly from the original.

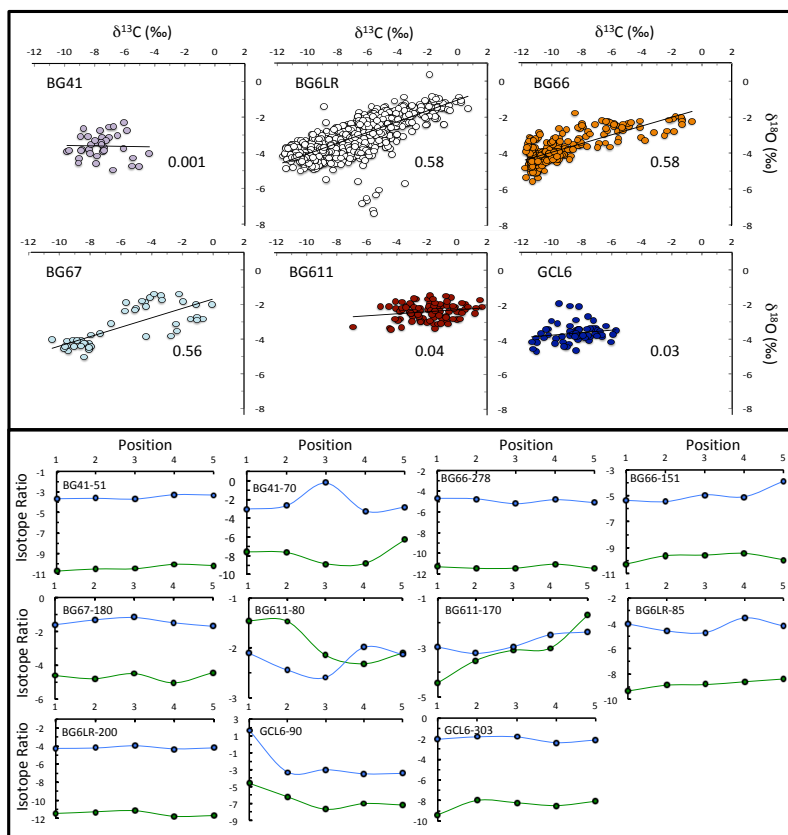


Figure 8. Hendy Tests of BG/GCL stalagmites. Top: Covariance plots of carbon and oxygen isotopic ratios. Correlation coefficients (r^2 values) are listed for each plot. High positive correlations have been identified as an indicator of non-equilibrium crystallization. Bottom: Oxygen (blue) and carbon (green) isotopic variations along the same growth layers with distance (listed in the upper left corner of each panel) from the stalagmite central growth axis. Progressive increases in $\delta^{18}\text{O}$ values have been interpreted to reflect disequilibrium crystallization. Limitations of the Hendy Tests are discussed in text.

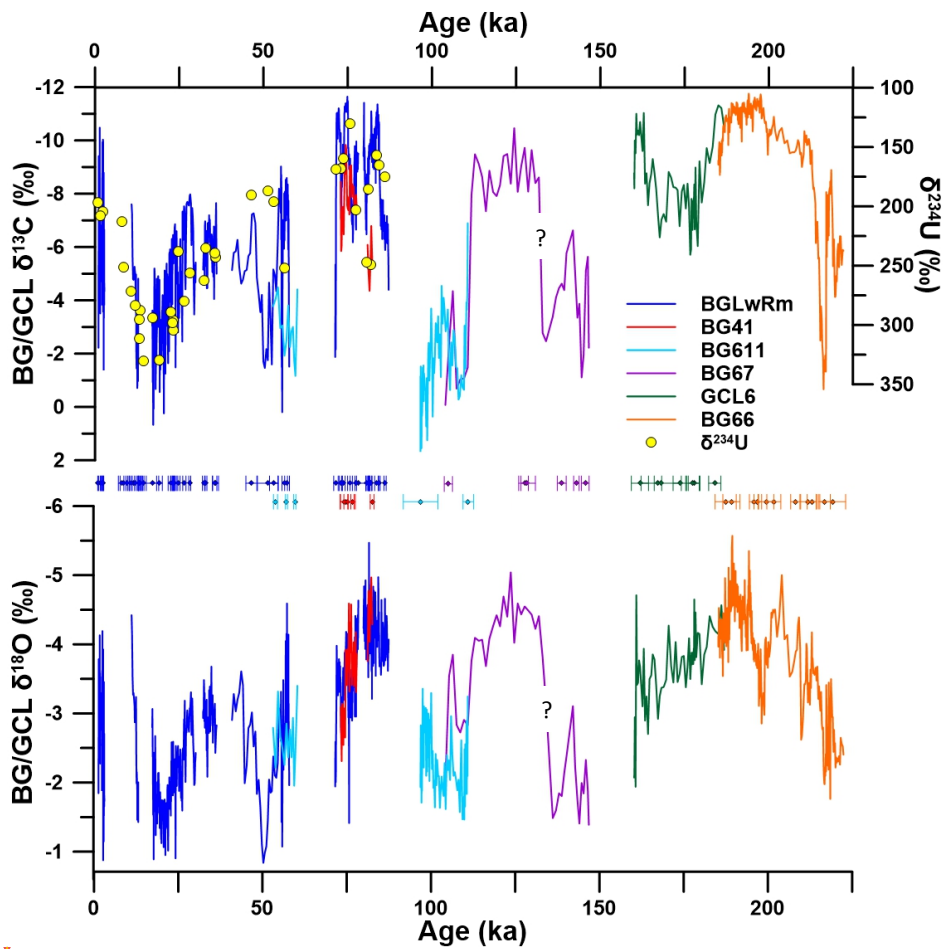
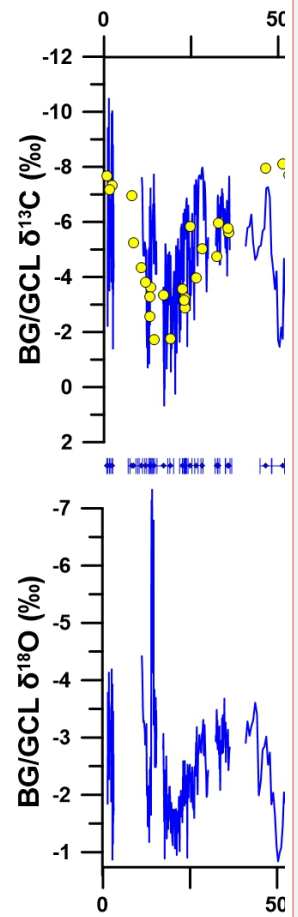


Figure 9. BG/GCL stalagmite isotopic time series. Carbon (top) and oxygen (bottom) isotopes, with each stalagmite presented in a different color. $\delta^{234}\text{U}$ values (yellow circles) for BG6LR are plotted against carbon isotope ratios (plots showing the $\delta^{234}\text{U}$ and $\delta^{13}\text{C}$ values of the other stalagmites are presented in the Supplemental Material). U/Th ages (with 2 s.d. errors) are also shown. The “?” at the MIS 6/5e transition denotes uncertainties associated with the continuity of this interval.

Rhawn Denniston 11/13/2018 4:16 PM



Deleted:

Unknown

Formatted: Font:(Default) Times New Roman

Unknown

Formatted: Font:(Default) Times New Roman

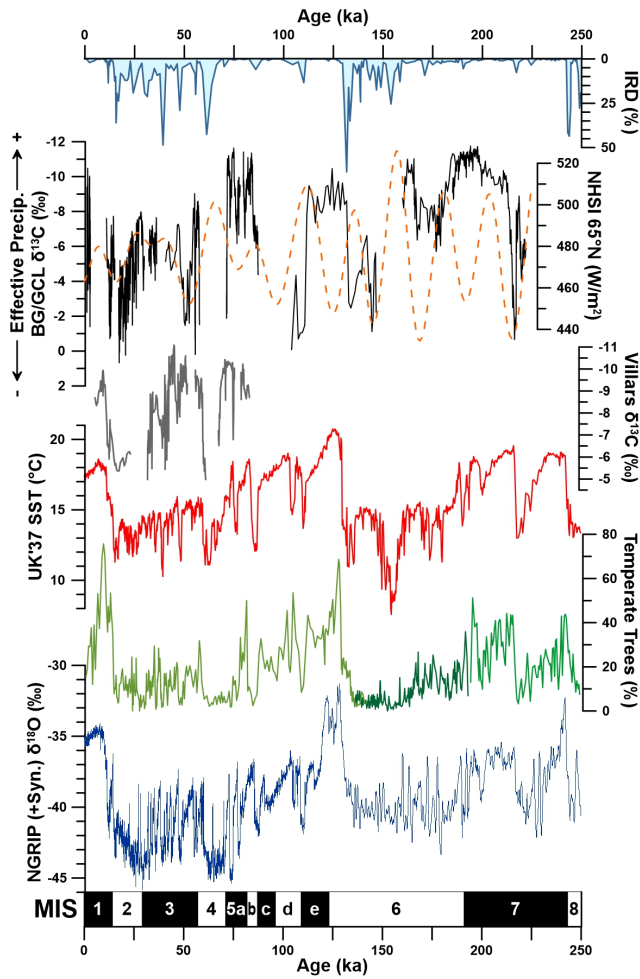


Figure 10. Comparison of Portuguese stalagmite hydroclimate proxies with regional and global climate records from the last two glacial cycles (A) Ice-rafted debris abundance from North Atlantic ODP Site 980 (McManus et al., 1999 using Hulu cave time scale as presented in Barker et al., 2011); (B) composite BG/GCL stalagmite carbon isotopic time series with NH summer insolation (Berger and Loutre, 1991); (C) Carbon isotopic time series from Villars Cave, southern France (Genty et al., 2003; Genty et al., 2006); (D) Alkenone-based Iberian margin SST reconstruction (core MD01-2443; Martrat et al., 2007); (E) Temperate forest pollen abundance from three closely spaced cores (MD01-2443: 250-194 ka (Roucoux et al., 2006; Tzedakis et al., 2004); MD01-2444: 194-136 ka (Margari et al., 2010; Margari et al., 2014); MD95-2042: 136-1 ka (Sánchez Goñi et al., 2008; Sánchez Goñi et al., 2013)); (F) NGRIP (0-122 ka) (North Greenland Ice Core Project members, 2004) and synthetic Greenland oxygen isotopic record (Barker et al., 2011) and (G) marine isotope stages.

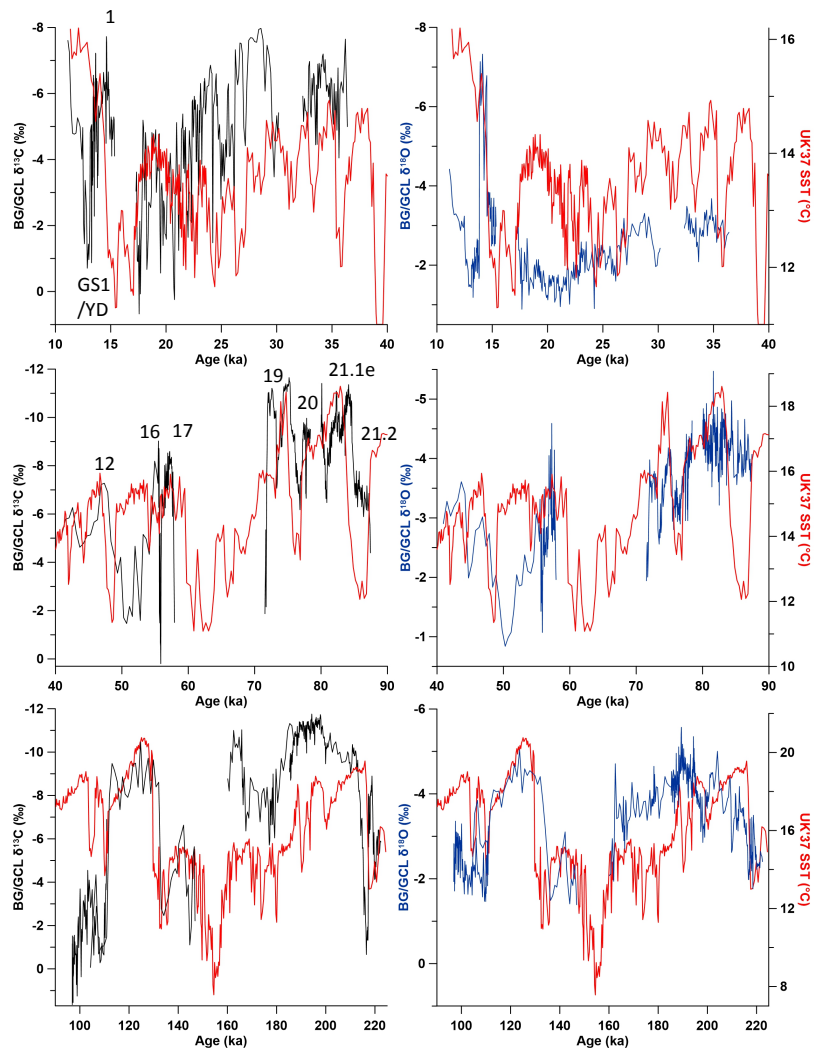


Figure 11. Iberian margin SST (red) and stalagmite carbon (black) and oxygen (blue) isotopes. Numbers denote select GI events using stratigraphic nomenclature of Rasmussen et al. (2014).

1247
1248
1249
1250
1251
1252
1253

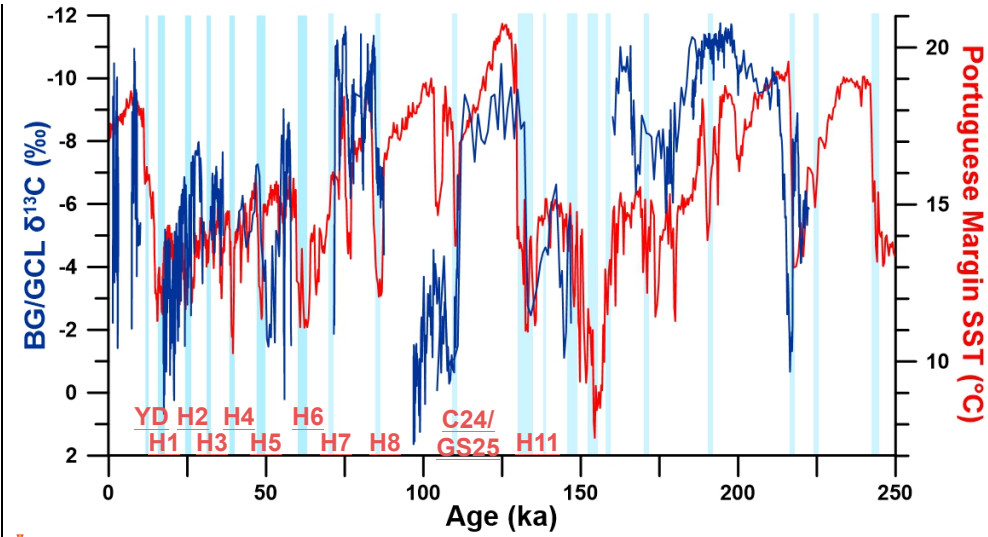


Figure 12. BG/GCL stalagmite carbon isotopic time series and Iberian margin SST. Light blue vertical rectangles denote North Atlantic cold events (some of which are labeled). Several interruptions in stalagmite growth coincide, within the errors of the stalagmite chronologies, with periods of depressed SST.

Rhawn Denniston 11/13/2018 4:16 PM

Deleted:

Unknown

Formatted: Font:(Default) Times New Roman

Unknown

Formatted: Font:(Default) Times New Roman

Table 1. U/Th Isotopic Ratios and ^{230}Th Ages

Stalagmite	Distance to Top (mm)	^{238}U (ng/g)	^{232}Th (pg/g)	$\delta^{234}\text{U}^a$ (corr'd)	Error ^b	$^{230}\text{Th}/^{238}\text{U}$ (activity)	Error	$^{230}\text{Th}/^{232}\text{Th}$ (ppm)	Error	Uncorrected Age (yr BP) ^c	Error (yr)	Corrected Age (yr BP) ^d	Error (yr)
BG41	67	148	2,892	524.7	2.2	0.779	0.0023	657.7	18.6	82,926	389	82,553	538
BG41	41	293	4,635	522.8	2.2	0.742	0.0030	773.8	8.5	77,026	463	76,724	486
BG41	21	217	1,858	566.6	3.1	0.748	0.0039	1,440.0	40.6	74,906	567	74,746	588
BG41	9	271	2,088	610.8	9.8	0.764	0.0073	1,635.6	22.3	74,392	1,135	74,253	1,142
BG66	266	85	6,980	698.6	9.3	1.283	0.0057	256.5	1.8	223,637	3,252	219,220	3,829
BG66	236	123	4,742	520.6	4.1	1.169	0.0030	500.0	4.0	217,460	1,752	216,719	1,780
BG66	218	101	3,132	532.4	3.1	1.174	0.0015	623.6	4.6	214,835	1,052	213,011	1,379
BG66	207	75	4,657	429.2	3.8	1.116	0.0025	298.1	1.7	215,891	1,580	211,971	2,478
BG66	194	68	2,003	499.5	3.1	1.149	0.0019	644.2	7.4	210,002	1,175	208,236	1,456
BG66	184	95	4,336	379.4	3.1	1.073	0.0025	386.6	3.6	204,768	1,460	201,770	2,063
BG66	154	104	2,193	443.5	2.6	1.100	0.0015	864.2	11.9	198,297	930	196,990	1,128
BG66	86	104	2,661	345.4	2.4	1.041	0.0016	672.5	8.4	197,507	994	195,798	1,298
BG66	54	76	995	564.2	6.2	1.159	0.0057	1,453.3	64.3	189,936	2,538	189,182	2,549
BG67	88	320	2,153	617.8	2.9	1.095	0.0043	2,689.7	51.5	146,174	1,146	145,802	1,158
BG67	79	195	2,799	485.8	2.3	1.014	0.0022	1,164.3	18.2	144,037	695	143,171	814
BG67	66	250	4,187	610.3	4.9	1.072	0.0046	1,057.4	12.7	139,735	1,279	138,803	1,350
BG67	44	162	4,858	484.7	2.4	0.969	0.0023	531.9	5.3	129,620	608	127,800	1,087
BG67	2	216	5,542	401.5	2.6	0.837	0.0039	538.0	5.1	107,150	843	105,501	1,168
BG611	173	119	11,744	202.6	3.5	0.801	0.0041	133.9	0.8	126,291	1,253	118,714	3,908
BG611	160	110	12,828	230.9	4.6	0.792	0.0044	112.1	0.7	118,672	1,277	109,828	4,469
BG611	30	122	16,801	251.3	5.0	0.762	0.0043	91.2	0.5	107,202	1,088	96,920	5,126
BG611	23	313	552	340.8	1.4	0.553	0.0024	5,168.2	353.7	59,726	345	59,608	350
BG611	12	248	2,233	356.2	1.6	0.547	0.0021	1,002.4	25.4	57,908	296	57,115	310
BG611	2	250	4,109	376.7	1.8	0.533	0.0021	535.0	5.9	54,959	284	53,887	604
BG6LR	1,623	72	133	175.0	1.5	0.631	0.0015	5,665.9	1,162	86,532	342	86,392	350
BG6LR	1,593	98	140	165.3	1.4	0.618	0.0014	7,166.0	1,764	84,748	318	84,639	324
BG6LR	1,574	74	905	156.6	1.6	0.615	0.0016	824.8	25.3	84,848	360	83,894	596
BG6LR	1,478	159	26	249.2	1.8	0.645	0.0021	63,745.2	114,070	82,068	428	82,056	428
BG6LR	1,464	166	1,138	246.8	1.5	0.641	0.0009	1,542.3	35.8	81,475	214	80,983	325
BG6LR	1,442	162	77	185.4	1.4	0.634	0.0039	21,885.5	13,015	81,442	396	81,407	396
BG6LR	1,375	112	220	202.9	1.5	0.602	0.0016	5,064.2	652.0	77,223	234	77,677	246
BG6LR	1,324	120	1,908	130.2	1.4	0.566	0.0060	585.8	15.3	77,213	330	75,946	712
BG6LR	1,283	132	1,019	159.5	2.0	0.566	0.0059	1,213.9	71.1	74,623	422	74,029	515
BG6LR	1,276	105	353	167.8	2.1	0.564	0.0037	2,766.4	298.1	73,512	425	73,254	444
BG6LR	1,246	83	1,232	168.7	1.4	0.561	0.0013	625.8	14.2	72,957	369	71,819	675
BG6LR	1,179	62	1,114	252.0	2.6	0.507	0.0071	464.4	15.9	57,877	465	56,584	792
BG6LR	1,174	77	2,544	196.0	2.2	0.474	0.0036	235.4	3.8	55,882	375	53,375	1,299
BG6LR	1,166	5	367	187.1	2.6	0.482	0.0041	100.4	1.6	57,644	524	51,517	3,066
BG6LR	1,153	81	3,460	190.7	2.2	0.433	0.0031	167.2	2.3	49,960	367	46,707	1,654
BG6LR	1,141	52	1,159	242.6	2.8	0.359	0.0039	266.4	10.4	37,626	449	36,016	918
BG6LR	1,138	55	750	239.5	1.8	0.352	0.0031	426.3	33.1	36,815	381	35,830	625
BG6LR	1,101	71	283	235.2	2.0	0.323	0.0034	1,344.2	198.7	33,449	272	33,161	310
BG6LR	1,093	70	472	262.1	2.1	0.327	0.0036	802.0	73.4	33,052	331	32,575	409
BG6LR	1,077	101	595	256.6	1.8	0.290	0.0039	810.6	63.4	28,851	193	28,431	287
BG6LR	1,068	85	1,034	280.0	1.4	0.285	0.0047	384.9	15.5	27,675	178	26,820	463
BG6LR	1,046	56	705	238.2	2.2	0.260	0.0063	339.0	19.7	25,911	265	24,993	531
BG6LR	1,026	123	2,093	304.1	1.9	0.262	0.0017	253.3	8.5	24,612	206	23,438	621
BG6LR	1,025	123	493	296.4	1.4	0.253	0.0017	1,041.2	151.0	23,814	175	23,538	226
BG6LR	1,019	80	377	298.5	2.1	0.252	0.0025	887.3	107.4	23,753	221	23,430	276
BG6LR	1,001	68	1,464	288.7	1.5	0.256	0.0058	196.1	4.3	24,291	156	22,789	765
BG6LR	944	76	1,896	329.3	2.1	0.233	0.0030	154.8	3.9	21,131	196	19,450	861
BG6LR	899	79	4,209	294.0	3.4	0.227	0.0066	70.6	1.3	21,074	283	17,360	1,863
BG6LR	883	91	233	330.3	2.0	0.168	0.0064	1,082.0	213.7	14,806	165	14,633	189
BG6LR	843	100	1,409	287.7	4.0	0.162	0.0023	190.4	6.7	14,718	164	13,738	516
BG6LR	827	103	332	295.0	2.9	0.152	0.0021	783.5	116.9	13,645	154	13,424	192
BG6LR	819	75	491	311.6	1.4	0.158	0.0018	400.0	22.8	14,032	123	13,587	255
BG6LR	783	95	525	283.8	2.2	0.141	0.0016	418.7	35.3	12,661	150	12,275	246
BG6LR	774	107	1,351	271.4	1.4	0.130	0.0014	169.8	5.7	11,795	119	10,901	463
BG6LR	759	135	4,177	251.5	1.5	0.121	0.0010	64.7	1.0	11,071	117	8,846	1,113
BG6LR	657	86	2,566	212.9	1.4	0.112	0.0010	62.1	0.9	10,540	96	8,326	1,106
BG6LR	139	172	323	204.2	1.7	0.031	0.0010	272.6	41.0	2,790	96	2,651	121
BG6LR	86	155	80	207.9	1.7	0.022	0.0007	720.9	312.3	1,987	62	1,949	67
BG6LR	10	122	43	196.7	18.9	0.014	0.0019	677.5	519.3	1,271	173	1,245	174
GCL6	439	91	2,815	76.3	2.3	0.862	0.0029	461.2	9.3	185,093	1,779	184,255	1,815
GCL6	394	86	3,009	125.7	2.0	0.881	0.0032	415.9	6.9	179,002	1,692	178,095	1,739
GCL6	335	70	4,579	82.7	3.0	0.856	0.0029	214.9	2.3	179,406	1,794	177,624	1,977
GCL6	292	75	2,61	78.2	2.9	0.845	0.0035	481.0	9.0	174,639	1,949	173,854	1,974
GCL6	256	116	1,019	86.2	2.2	0.836	0.0020	1,574.3	71.8	167,617	1,102	167,382	1,105
GCL6	165	94	2,507	122.4	4.2	0.847	0.0049	526.3	13.4	162,712	2,368	162,022	2,550

^a $\delta^{234}\text{U}_{\text{meas/d}} = [(^{234}\text{U}/^{238}\text{U})_{\text{meas/d}} / (^{234}\text{U}/^{238}\text{U})_{\text{eq}} - 1] \times 10^3$, where $(^{234}\text{U}/^{238}\text{U})_{\text{eq}}$ is secular equilibrium activity ratio: $\lambda_{238}/\lambda_{234} = 1.0$. Values reported as permil.

^b Errors are at the 2 σ level.

^c Present is defined as the year AD 1950.

^d Initial $^{230}\text{Th}/^{232}\text{Th}$ atomic ratio of $13.5 \times 10^{-6} \pm 6.75 \times 10^{-6}$ used to correct for unsupported ^{230}Th in BG stalagmites. GCL stalagmites use $4.4 \times 10^{-6} \pm 2.2 \times 10^{-6}$.

Stalagmite	Distance to Top (mm)	^{238}U (ng/g)	^{232}Th (pg/g)
BG41	67	148	2,892
BG41	41	293	4,635
BG41	21	217	1,858
BG41	9	271	2,088
BG66	266	85	6,980
BG66	236	123	4,742
BG66	218	101	3,132
BG66	207	75	4,657
BG66	194	68	2,003
BG66	184	95	4,336
BG66	154	104	2,193
BG66	86	104	2,661
BG66	54	76	995
BG67	88	320	2,153
BG67	79	195	2,799
BG67	66	250	4,187
BG67	44	162	4,858
BG67	2	216	5,542
BG611	173	119	11,744
BG611	160	110	12,828
BG611	30	122	16,801
BG611	23	313	552
BG611	12	248	2,233
BG611	2	250	4,109
BG6LR	1,623	72	133
BG6LR	1,593	98	140
BG6LR	1,574	74	905
BG6LR	1,478	159	26
BG6LR	1,464	166	1,138
BG6LR	1,442	162	77
BG6LR	1,375	112	220
BG6LR	1,324	120	1,908
BG6LR	1,283	132	1,019
BG6LR	1,276	105	353
BG6LR	1,246	83	1,232
BG6LR	1,179	62	1,114
BG6LR	1,174	77	2,544
BG6LR	1,166	5	367
BG6LR	1,153	81	3,460
BG6LR	1,141	52	1,159
BG6LR	1,138	55	750
BG6LR	1,101	71	283
BG6LR	1,093	70	472
BG6LR	1,077	101	595
BG6LR	1,068	85	1,034
BG6LR	1,046	56	705
BG6LR	1,026	123	2,093
BG6LR	1,025	123	493
BG6LR	1,019	80	377
BG6LR	1,001	68	1,464
BG6LR	944	76	1,896
BG6LR	899	79	4,209